REPUBLIC OF TURKEY

YILDIZ TECHNICAL UNIVERSITY

GRADUATE SCHOOL OF NATURAL AND APPLIED SCIENCES

DESIGN OF FLUXGATE MAGNETOMETER

SERCAN TANRISEVEN

MSc. THESIS

DEPARTMENT OF ELECTRONICS AND COMMUNICATIONS ENGINEERING

PROGRAM OF COMMUNICATION ENGINEERING

ADVISER

ASST. PROF. DR. REVNA ACAR VURAL

İSTANBUL, 2017

REPUBLIC OF TURKEY

YILDIZ TECHNICAL UNIVERSITY

GRADUATE SCHOOL OF NATURAL AND APPLIED SCIENCES

DESIGN OF FLUXGATE MAGNETOMETER

A thesis submitted by Sercan TANRISEVEN in partial fulfillment of the requirements for the degree of **MASTER OF SCIENCE** is approved by the committee on 25.05.2017 in Department of Electronics and Communications Engineering, Communication Engineering Program.

Thesis Adviser

Asst. Prof. Dr. Revna ACAR VURAL

Yıldız Technical University

Co- Adviser

Assoc. Prof. Dr. Uğur TOPAL

TUBITAK

Approved By the Examining Committee

Asst. Prof. Dr. Revna ACAR VURAL

Yıldız Technical University _____

Assoc. Prof. Dr. Nurhan TÜRKER TOKAN, Member

Yıldız Technical University _____

Asst. Prof. Dr. Yiğit Dağhan GÖKDEL, Member

İstanbul Bilgi University _____

This study was supported by the Scientific and Technological Research Council of Turkey (TUBITAK) Grant No: 113F192.

ACKNOWLEDGEMENTS

I would like to thank my thesis advisor Asst. Prof. Dr. Revna ACAR VURAL. She always motivated me with a positive approach with infinite trust and made me do this study despite all my mistakes and deficiencies.

I would also like to thank the experts who were involved in for this research project. Firstly Dr. Uğur TOPAL and Dr. Cengiz BİRLİKSEVEN. Without their theoretically and practically helps, the thesis survey could not have been done. I would also like to thank TUBITAK UME Magnetic Laboratory for their support and assistance to their employees. This study was supported by the Scientific and Technological Council of Turkey (TUBITAK) Grant No: 113F192

Finally, I must express my very profound gratitude to my parents and especially my wife Zulhice MEHMEDİ for providing me with unfailing support and continuous encouragement throughout my years of study and through the process of researching and writing this thesis. This accomplishment would not have been possible without them.

Thank you.

May, 2017

Sercan TANRSEVEN

TABLE OF CONTENTS

Page

LIST OF ABBREVIATIONS vii

LIST OF FIGURES ix

ABSTRACT xi

ÖZET xiii

CHAPTER 1

INTRODUCTION 1

1.1 Fundamentals of Magnetism 1

1.2 Magnetometers 2

1.2.1 Inductive Pick-Up Coils 3
1.2.2 Hall Effect Magnetometers 3
1.2.3 Magnetoresistive Magnetometers 3
1.2.4 SQUID Magnetometer 4
1.2.5 Vibrating Sample Magnetometer 4
1.2.6 Fluxgate Magnetometers 5
1.2.7 Rod Core Fluxgate Sensors 6
1.2.8 Ring Core Fluxgate Sensors 7
1.2.9 Race Track Core Fluxgate Sensors 7

1.3 Literature Review 8

1.3.1 Researches on Fluxgate sensors 8
1.3.2 Researches on Fluxgate magnetometer electronics 10
1.3.3 Fluxgate magnetometers designed for use in space missions 12
1.3.4 Fluxgate magnetometers designed for use in different disciplines 14

CHAPTER 2

FLUXGATE SENSOR THEORY AND IMPLEMENTATION 16

2.1 Design of Excitation Coil 16
2.2 Design of Pick-Up Coil 19
2.3 Working Principles of Ring Core Fluxgate Sensor 20

CHAPTER 3

LOCK-IN AMPLIFIER DESIGN 23

3.1 Introduction to Lock-In Amplifier 23
3.2 Fundamentals of Lock-In Amplifiers 25
3.3 Analog Lock-In Amplifier Design 26
3.4 Digital Lock-In Amplifier 27

CHAPTER 4

FLUXGATE MAGNETOMETER DESIGN 33

4.1 General Design Approach of Fluxgate Magnetometer 33
4.2 Fluxgate Magnetometer Driver Circuit 34
4.3 Fluxgate Magnetometer Pick-Up Circuit 35
4.4 Application 42
4.4.1 TUBITAK UME Fluxgate Magnetometer Application 42

CHAPTER 5

CONCLUSION AND FUTURE WORKS 46

REFERENCES 48

CURRICULUM VITAE 52

LIST OF ABBREVIATIONS

3D	Three Dimension
AAF	Anti Aliasing Filter
AC	Alternating Current
ADC	Analog Digital Converter
ALIA	Analog Lock-In Amplifier
AMR	Anisotropic Magneto Resistance
ASIC	Application Specific Integrated Circuit
BC	Before Christ
BPF	Band Pass Filter
DAC	Digital Analog Converter
DC	Direct Current
DLIA	Digital Lock-In Amplifier
DMA	Direct Memory Access
dsPIC	ds Series Peripheral Interface Controller
DSP	Digital Signal Processing
EMR	Extraordinary Magneto Resistance
ESA	European Space Agency
FGM	Fluxgate Magnetometer
FIR	Finite Impulse Response
FPGA	Field Programmable Gate Array
GMR	Giant Magneto Resistance
LCD	Liquid Cyrstal Display
LPF	Low Pass Filter
MSc.	Master of Science
NASA	National Aeronautics and Space Administration
NDT	Nondestructive Testing
NiFe	Nickel Iron Alloy
PCB	Printed Circuit Board
PEEK	Polyether Ether Ketone
PSD	Phase Sensitive Detection
RC	Resistance Capacitor
SQUID	Superconducting Quantum Interference Device
SMPS	Switch Mode Power Supply

TMR	Tunnel Magneto Resistance
UXO	Unexploded Ordnance
UME	Ulusal Metroloji Ensititüsü
VHDL	VHSIC Hardware Description Language
VSM	Vibrating Sample Magnetometer

LIST OF FIGURES

Page

Figure 1.1 MAG3110 magnetoresistive sensor based 3D magnetometer chip 3
Figure 1.2 MPMS3 SQUID magnetometer 4
Figure 1.3 DMS Vibrating Sample Magnetometer 5
Figure 1.4 Ring Core Fluxgate Magnetometer System Implementation 6
Figure 1.5 Dual Rod Core Fluxgate Sensor Structure 6
Figure 1.6 Ring Core Fluxgate Sensor Structure Race Track Fluxgate Sensors 7
Figure 1.7 Race Track Core Fluxgate Sensor Structure 8
Figure 2.1 Ring core Fluxgate sensor excitation coil 16
Figure 2.2 A sample of Metglas material 17
Figure 2.3 Hysteresis loops of Metglas 2714A material 18
Figure 2.4 Ring core Fluxgate sensor pick up coil 19
Figure 2.5 Winding of pick-up coil 20
Figure 2.6 Mathematical Model of Metglas 2714A's B-H curve 21
Figure 2.7 Excitation (orange) and Pick-up (blue) signal of Fluxgate Sensor 22
Figure 3.1 A standard lock-in amplifier for laboratory use 24
Figure 3.2 Single-phase basic lock-in amplifier circuit diagram 24
Figure 3.3 Basic two-phase lock-in amplifier circuit diagram 24
Figure 3.4 Single-phase PSD, lock-in amplifier scheme 26
Figure 3.5 Analog Fluxgate magnetometer block diagram 27
Figure 3.6 0 and 90 degree phase, in phase and quadrature phase reference signals 28
Figure 3.7 Multiplication with input signal and reference signal 29
Figure 3.8 FIR filtering results with $\pi / 3$ phase difference 30
Figure 3.9 Two-time filtering FIR filter outputs with 0 degree phase difference 30
Figure 3.10 Two-stage filter outlet with $\pi / 4$ phase difference 31

Figure 3.11 DLIA digital circuit schematic 31
Figure 3.12 DLIA algorithm flow chart in MATLAB and C++ 32
Figure 4.1 Digital Fluxgate Magnetometer (a) Circuit diagram (b) Main blocks 34
Figure 4.2 Driver signal of Fluxgate sensor 35
Figure 4.3 Second Harmonic Signals versus External DC Magnetic Field 36
Figure 4.4 Negative value of pick-up signal in zero phase 37
Figure 4.5 Positive value of pick-up signal at zero phase 37
Figure 4.6 Entire Fluxgate magnetometer circuit schematic 38
Figure 4.7 The entire system image of the designed Fluxgate Magnetometer 38
Figure 4.8 Designed Fluxgate magnetometer's circuit connections 39
Figure 4.9 Fluxgate magnetometer sensitivity measurement setup 40
Figure 4.10 Fluxgate magnetometer noise level measurement setup 41
Figure 4.11 First generation UME Fluxgate magnetometer (a) Sensitivity (b) Noise measurements 43
Figure 4.12 World magnetic field oscillations in the UME building controlled area from September 12 to 17 44
Figure 4.13 World Magnetic Field oscillations in the UME building controlled zone from December 21 to 29 45

ABSTRACT

DESIGN OF FLUXGATE MAGNETOMETER

Sercan TANRISEVEN

Department of Electronics and Communications Engineering

MSc. Thesis

Adviser: Asst. Prof Dr. Revna ACAR VURAL

Co-adviser: Assoc. Prof. Dr. Uğur TOPAL

The import of high-tech products increases the external dependency of countries. In this thesis study, fluxgate magnetometer design, which has the potential to use many fields from defense industry, space researches, basic science researches, material characterization techniques, has been done. This work was supported by TUBITAK National Metrology Institute. Fluxgate magnetometer design study includes Fluxgate sensor design, digital lock-in amplifier design and digital Fluxgate magnetometer design.

In this thesis, a sensitive and low cost magnetometer was designed to measure natural earth magnetic field value between ± 0.6 G. Using microcontrollers with a phase detection code technique system was realized, unlike using conventionally lock-in amplifier. The sensor was driven by excitation signal whose frequency is 1.086 kHz and magnitude is 1.31 V. Eventually, the direction and the magnitude of DC magnetic field is successfully determined with the fluxgate magnetometer. All these studies were carried out and a large literature survey was conducted and a great deal of knowledge was gained on this highly potent subject which was not much interested in our country.

Key words: Fluxgate magnetometer, lock-in amplifier, magnetic field measurement, fluxgate sensor, magnetometer electronics.

ÖZET

FLUXGATE MANYETOMETRE TASARIMI

Sercan TANRISEVEN

Elektronik ve Haberleşme Mühendisliği

Yüksek Lisans Tezi

Tez Danışmanı: Yrd.Doç. Dr. Revna ACAR VURAL

Eş Danışman: Doç. Dr. Uğur TOPAL

Yüksek teknolojili ürünlerin ithalatı, ülkelerin dışa bağımlılığını arttırmaktadır. Bu tez çalışmasında, savunma sanayi, uzay araştırmaları, temel bilim araştırmaları, malzeme karakterizasyon tekniklerinden pek çok alanı kullanma potansiyeline sahip olan Fluxgate manyetometre tasarımı yapılmıştır. Bu çalışma TÜBİTAK Ulusal Metroloji Enstitüsü tarafından desteklenmiştir. Fluxgate manyetometre tasarım çalışması, Fluxgate sensör tasarımı, dijital kilitlemeli amplifikatör tasarımı ve dijital Fluxgate manyetometre tasarımını içerir.

Bu tezde, ± 0.6 G aralığında bulunan doğal manyetik alan değeri ölçebilmek için hassas ve düşük maliyetli bir manyetometre tasarlanmıştır. Geleneksel kilitlemeli amplifikatörün kullanılmasının aksine, mikro denetleyiciler ile gerçeklenmiş bir faz tespit kod tekniği ile sistem gerçekleştirilmiştir. Sensör, frekansı 1.086 kHz ve genliği 1.31 V olan uyarılma sinyali ile sürülmüştür. Sonunda, DC manyetik alanın yönü ve büyüklüğü, Fluxgate manyetometre ile başarıyla belirlenmiştir. Bütün bu çalışmalar yürütülürken büyük bir literatür taraması yapılmış ve ülkemizde henüz pek çalışılmamış, yüksek potansiyelli bu konu üzerine bilgi birikimi sağlanmıştır.

Anahtar Kelimeler: Fluxgate manyetometre, kilitlemeli yükselteç, manyetik alan ölçümü, fluxgate sensör, manyetometre elektroniği

CHAPTER 1

INTRODUCTION

1.1 Fundamentals of Magnetism

Magnetism has attracted the attention of people since ancient times, and the first academic studies in this regard began in about 6th century BC. In the 11th century, the Chinese also found an effective method of using the magnetic field - using lodestone - in daily life. This invention has been compass, and has become one of the most important inventions that have shaped the history of the world. Along with scientific knowledge, significant improvements in the magnetic field occurred in the early 19th century. The relationship between electricity and magnetism was first investigated by Hans Christian Oersted. Scientist such as Ampere, Gauss, Biot, Savart, Faraday and Maxwell have also made studies that reveal the duality of electric current and magnetic field. Along with the Biot-Savart law, differential magnetic field generated by the current flowing through the linear wire is expressed as shown in the following equation.

$$\mathrm{B(r)} = \frac{\mu_0}{4\pi} \oint \frac{I\mathrm{dl\ x\ r'}}{|\mathrm{r'}|^3} \tag{1.1}$$

Ampere has established the relationship between the electric current passing through that loop by the integral of the magnetic field along a closed loop. This law is one of the basic laws of electromagnetism.

$$\oint \vec{\mathrm{B}}.\,\mathrm{d}\vec{\mathrm{l}} = \mu_0 \iint \vec{\mathrm{J}}\mathrm{d}\vec{\mathrm{S}} \tag{1.2}$$

Gauss's law of magnetism says that magnetic flux along a closed surface is zero. This law states that magnetic field lines form a closed loop.

$$\oiint \vec{B}.d\vec{S} = 0 \quad (1.3)$$

Faraday's induction law discloses that the induced voltage across a closed circuit is related to the change in magnetic flux density passing through that circuit.

$$V_{ind} = \oint \vec{E}.d\vec{l} = -\frac{d}{dt}\iint \vec{B}.d\vec{S} \quad (1.4)$$

James Clerk Maxwell explained that by combining all of these laws, all of them are the laws that make up the basis of electromagnetism. So four Maxwell equations have emerged that define electromagnetism. These equations are given below respectively.

$$\oiint \vec{E}.d\vec{S} = \frac{1}{\varepsilon_0}\iiint \rho dV \quad (1.5)$$

$$\oiint \vec{B}.d\vec{S} = 0 \quad (1.6)$$

$$\oint \vec{E}.d\vec{l} = -\frac{d}{dt}\iint \vec{B}.d\vec{S} \quad (1.7)$$

$$\oint \vec{B}.d\vec{l} = \mu_0 \iint \vec{j}dS + \mu_0\,\varepsilon_0 \frac{d}{dt}\iint \vec{E}.d\vec{S} \quad (1.8)$$

The above mentioned mathematical correlations helped to develop the technologies we use today. It is only possible to measure and evaluate the magnetic field which is the main idea of the thesis based on mathematical expressions.

In this thesis, we aimed to design fluxgate magnetometers which have many uses of the field to reduce the technological external dependence of our country. An innovative, low-cost and simple fluxgate magnetometer was built on this topic.

1.2 Magnetometers

Common name given to devices that measure the intensity and / or direction of a magnetic field. Magnetic field measurement may be needed for a variety of purposes. Therefore, various magnetometers with different operating principles have been developed. The various types of magnetometers are listed below.

- Inductive Pick-Up Coils
- Hall Effect magnetometer
- Magnetoresistive Magnetometers

- Fluxgate Magnetometer
- SQUID Magnetometer
- Vibrating Sample Magnetometer

1.2.1 Inductive Pick-Up Coils

This type of magnetometer is a passive sensor structure that only detects the changing magnetic fields according to the Ampere law. A changing magnetic field causes flux on a closed conductive path and the magnetic field is sensed. Another name is "Search Coil". It is used in underground detectors.

1.2.2 Hall Effect Magnetometers

Hall effect sensors generate voltage, based on the deflection of the charged particles in the magnetic field. It provides the relationship between magnetic field and voltage. They can be used in chips because they can be produced in very small sizes. This sensor structure is also used to design a magnetometer [1].

1.2.3 Magnetoresistive Magnetometers

These types of magnetometers are realized by special materials that change their electrical resistances when exposed to a magnetic field [2].

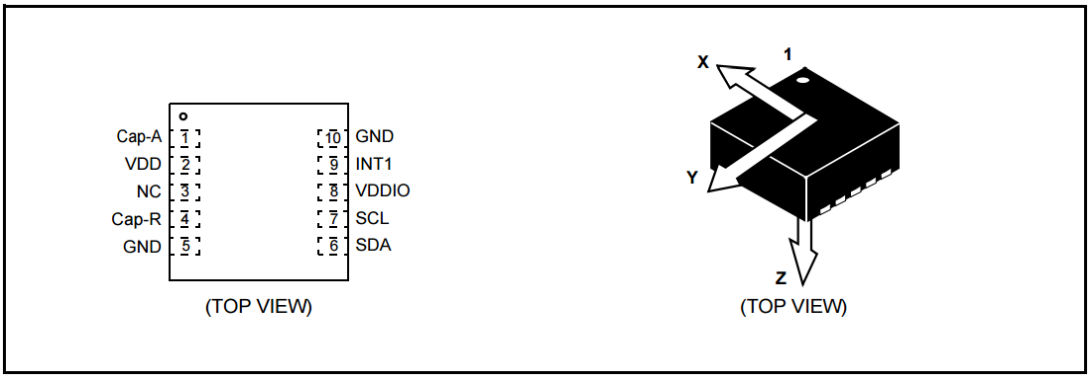


Figure 1.1 MAG3110 magnetoresistive sensor based 3D magnetometer chip [1]

When the resistance change is measured accurately, information about the magnetic field is obtained. These materials have been developed over time to develop

magnetoresistive sensors and magnetometers with the name of AMR, GMR, TMR, and EMR .

1.2.4 SQUID Magnetometer

SQUID magnetometer is a magnetometer containing Josepson junctions. This magnetometer allows the superconducting rings to measure very low magnitude magnetic fields under low temperature. Bulky structure permits use only in laboratory conditions [3].



Figure 1.2 MPMS3 SQUID magnetometer [4]

1.2.5 Vibrating Sample Magnetometer

It is a magnetometer developed to determine the magnetic properties of materials. The material sample is placed between two coils forming a DC magnetic field and is sinusoidally vibrated. When this change is analyzed the magnetic characterization of the material is made. This system is called VSM [5].



Figure 1.3 DMS Vibrating Sample Magnetometer [6]

1.2.6 Fluxgate Magnetometers

Fluxgate magnetometers are similar to searching coil magnetometers. Because they are based on the same physical phenomenon. Searching coil magnetometers detect external magnetic fields with a single passive coil. Fluxgate magnetometers have two bobbins. One of the coils is used as the excitation-the source of the magnetic field, while the other coil acts as the pick-up coil. Fluxgate magnetometers measures both AC and DC very low magnetic field with high sensitivity, reliability and robustness [7]. They are widely used in defense applications, industrial devices, space, navigation and medical implementations [8]. Conventionally, three main fluxgate sensor structures such as ring core, rod type and race track are preferred in the literature. The ring core fluxgate sensor serve lower noise level performance than the others.

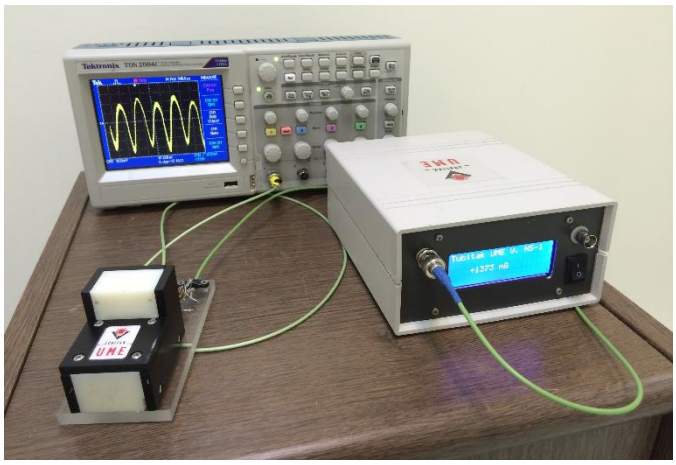


Figure 1.4 Ring Core Fluxgate Magnetometer System Implementation

1.2.7 Rod Core Fluxgate Sensors

Rod-type fluxgate sensors are obtained by wrapping the excitation and detection coils around a bar-shaped soft magnetic material. Immunity to the magnetic field is weak because they do not form a structurally closed cycle. Since the tip portions are open, they emit magnetic fields. On the other hand, the measurements provide higher resolution than other types of fluxgate sensors [9].

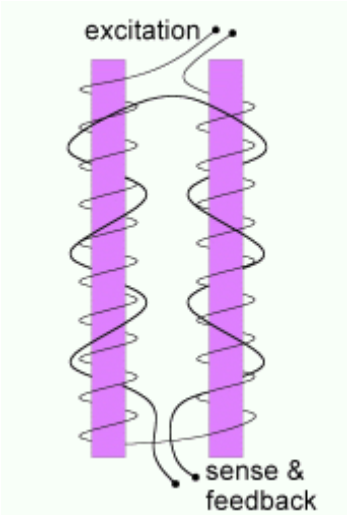


Figure 1.5 Dual Rod Core Fluxgate Sensor Structure [10]

1.2.8 Ring Core Fluxgate Sensors

Ring core sensors are sensors in which the excitation coil is wound in a toroidal form and placed in a solenoid coil. The toroidal core is selected from special core materials made from soft magnetic material. These materials are materials that react very sensitively to the magnetic field. Working principle resembles dual rod core fluxgate sensors. However, since they have closed loop structures, they have higher noise immunity and release less magnetic fields. This reduces the amount of power required to drive and saturate such sensors. The disadvantages of ring core fluxgate sensors are less sensitivity than rod core sensors and the effect of demagnetization is high. The demagnetization effect or factor is a relationship between the applied magnetic field and the amount of magnetization of the material. The demagnetization factor is a constant that varies depending on the geometry of the magnetized material. Power consumption is less. High immunity to noise and mechanical robustness make ring core fluxgate sensors more advantageous than other sensors. In general commercial and industrial fluxgate magnetometers are realized with ring core sensors [9].

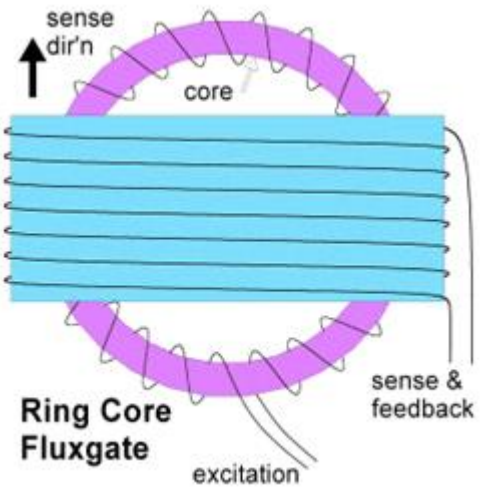


Figure 1.6 Ring Core Fluxgate Sensor Structure [11]

1.2.9 Race Track Core Fluxgate Sensors

Race track core fluxgate sensors are a special form of ring core sensors. This design was made to reduce the high demagnetization effect of ring core sensors. The working principle is the same as the ring core sensor. With this geometry, the demagnetization effect is reduced and the immunity to the vertical areas is increased. However, offset

adjustment and production of such sensors is difficult. This sensor structure is preferred in the production of PCB type magnetic sensors.

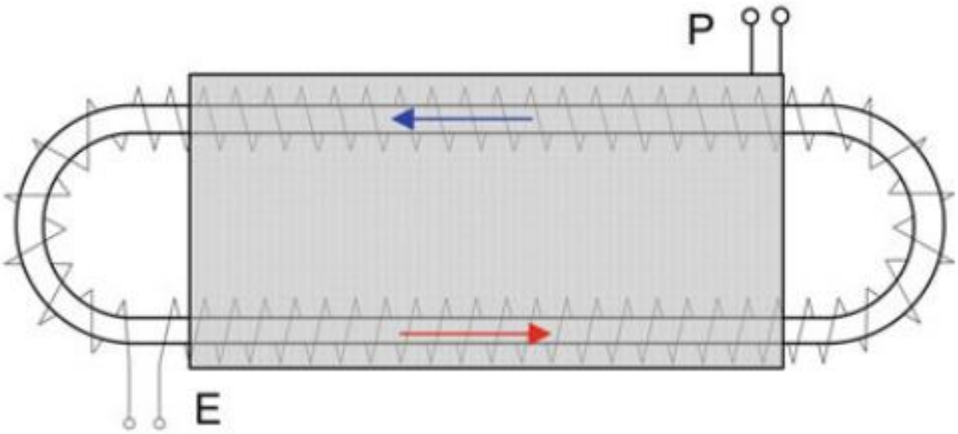


Figure 1.7 Race Track Core Fluxgate Sensor Structure [12]

1.3 Literature Review

The literature search on the Fluxgate magnetometer is divided into four main parts and the topic distributions are grouped. In this context, academic approaches related to fluxgate magnetometers in the literature are as follows.

1.3.1 Researches on Fluxgate sensors

The articles in this title have focused on the investigation of various aspects of the Fluxgate sensor design. Miniaturization of Fluxgate sensor, improvement of noise and / or offset performance, investigation of response to temperature change, new approaches on general design, and articles on new materials used in magnetic sensor construction.

In 2006 an article was published that presented studies to improve the efficiency of the excitation (drive) signal [13]. In this article, the current form of the drive signal and the capacity value connected to the drive coil have been studied. Lower power consumption is targeted by increasing drive signal efficiency. Excitation signal in sinusoidal form was studied. The appropriate current form for the drive coil with nonlinear character is numerically calculated. Thus the power of an 'untuned' excitation coil is measured between 0.3-0.5 W.

In the same year an article was published on the 'racetrack fluxgate sensor' about the noise reduction on the output signal [14]. This algorithm is run on double harmonics at the output of the fluxgate sensor. This algorithm reduces the noise of an output signal digitized by the ADC. However, since this process also reduces the sensitivity of the sensor, this algorithm has been implemented on the 4th harmonic and the noise reduction has been achieved.

In 2008, an article was published by the LVIV Center for Institute for Space on the thermal drift, noise, excitation signal and long-term stability of racetrack fluxgate sensors [15]. As a result of the research, Co68Fe3Cr3Si15B12 alloy crystal is proposed for the lowest noise level. The 'Macor' material has been tested and recommended as a mechanical structure for long term sensor stability. A sinusoidal form is proposed as a form of drive current signal. For maximum performance, the drive circuit is resonated at the frequency of the excitation signal.

A published article in 2009 examined the crossfield effect in magnetic sensors.[16] The effect of the magnetic field components perpendicular to the direction in which the sensors measure is an important problem, which is called the crossfield effect. Many magnetic field sensors are affected by this. In the study performed, error graphs are plotted under the crossfield effect of AMR and fluxgate sensors. For Fluxgate sensors, the cross field effect is typically below 5 nT for Vacquier and race track sensors and below 20 nT for ring-core sensors, all of which are measured in the earth magnetic field range. These sensors are very sensitive to cross areas and even areas in the same direction. Severe magnetic fields, the magnetization of the sensor can be changed irreversibly. The crossfield effect causes a crossfield effect error of around 5nT on the Vacquier and race track sensor and around 20 nT on the ring core sensors. Therefore, these sensors must be driven with alternating signals. In addition, the feedback compensation technique is another factor that reduces the crossfield effect error.

Feedback circuits are used to increase the measurement range of the fluxgate sensors, but feedback mechanisms and their materials can have effects on the sensor element. One of these effects, noise, was addressed in two articles published in 2010. A three-dimensional, vector feedback circuit surrounds the cube-shaped sensor [17]. The glue material filling between the cube and the sensor element is selected from a heat-

insulating material. In this way the noise from the thermal changes is reduced. The 40x40x47 140 g weight 3D sensor and feedback packages have been implemented in a compact approach. In another article, the sensor was given a 'feedback current' to the drive coil, without adding an extra feedback coil structure [18]. This way the measurement range is increased. In this way, the measurement range has been expanded even if not as much as the additional feedback structure.

Barkhausen noise and mechanical stress problem which is one of the disadvantages of ring core sensors compared to rod type sensors. According to an article published in 2012, sensors made of metallic glass ribbons wrapped around a hoop to form a loop were produced [19]. With this technique, the lowest noise ring core sensors of 12 mm diameter are obtained. The sensors used in this thesis are also produced with this technique. The large and cumbersome nature of the fluxgate sensors has caused them to experiment in micro-dimensions.

For this purpose, in 2014 a micro fabricated fluxgate sensor was realized by spraying NiFe on a thin film [20]. The noise of the sensors in this structure is quite high, but it has enabled the sensors to be driven in the dimensions of Mhz. Since they are realized with magnetic core material in a small amount, the amount of current required for deep saturation can be reduced to 6mA and very low power fluxgate sensors are realized on thin film.

1.3.2 Researches on Fluxgate magnetometer electronics

The articles in this chapter deal with the circuit design of the fluxgate sensor designed to generate the drive signal and process the pick-up signal. In this context, analog, digital or hybrid magnetometer electronics designs have been studied. In addition, studies on the most critical elements of magnetometer electronics, such as the lock-in amplifier and the feedback circuit, have been investigated.

In Fluxgate magnetometer designs, electronic structures called lock-in amplifiers are used to measure very low magnetic fields with high accuracy. This structure senses the signal even if it is lost in the noise.[21] A review of the signal filtering at the output of the lock-in amplifier circuit in a published article in 2010 was conducted. Usually a low pass filter is added to the lock-in amplifier output at 0-10 Hz band and the DC

component is filtered. In this study, the signal obtained by filtering twice the excitation frequency was analyzed. As a result, even the signals below -20 dB can be recovered by 2nd harmonic filtering. It is certain that this technique will introduce more signal processing load than the DC filtering technique. However, this trade off can be accepted when necessary.

In another case, the lock-in amplifier output signal is analyzed to be cleaner by increasing the amplitude of the lock-in amplifier reference signal. It has been shown in the same article that the lock-in amplifier output signal will cause more accurate measurement results if the sampling frequency is increased [22].

In this thesis, although DC magnetic field measurements are emphasized, AC magnetic field measurements were made with dual lock-in amplifier structure in the literature. The disadvantage of this structure is the implementation of the lock-in amplifiers with the band as much as the bandwidth of the signal to be measured .

Lock-in amplifier design has the obligation to multiply the input and reference signals. This leads to some difficulties in designing the lock-in amplifier as an embedded chip. The higher the sampling frequency, the more precise the lock-in amplifier will be. Thus, all of the digitally generated lock-in amplifier reference signal can be used to multiply the sampled analog signal by acceleration algorithms.

A study published in 2012 on this issue has been done. 20 samples taken for a period were reduced to 4 symmetrical samples and a simpler digital lock-in amplifier design was realized by reducing the process load. The disadvantage of this approach is that the very high accuracy performance expected from the lock-in amplifiers is lower [23].

In 2013, the dsPIC series of microcontrollers have been studied on lock-in amplifier design for embedded lock-in amplifier. It has been observed that the ADC sampling frequency is directly proportional to the noise immunity. It is predicted that the simulations in MATLAB will give approximately the same performance as the embedded lock-in amplifier design [24].

In 2014, a lock-in amplifier was implemented with the TMS320 series DSP. It has also been shown that it can be a compact design with low power consumption in this way. The DSP-powered lock-in amplifier consumes 22mW [25].

The fluxgate magnetometers have been realized as digital, analog or hybrid and various methods have been used for this. There are MSc. theses written on this subject. In these theses, magnetometer designs are generally made entirely analogue or digital with FPGA. In 2014, a digital magnetometer with a simple ring core sensor, a hybrid digital design with FPGA and microcontroller, was used to study the magnetosphere effect of solar storms [26].

One of the biggest problems with rod core fluxgate sensors is the offset problem. Analyzes have been made to solve this problem and various methods have been proposed. One of them has been to use the offset of the drive signal to apply a sensor with non-zero DC offset to zero the general offset. In this technique, the DC offset of the drive signal is periodically added and subtracted in equal amounts. This has minimized offset degradation due to sensor design and temperature variation, but it is unlikely to be used in space applications because it increases the total power consumption [27].

In the 2014, the offset problem of sensors exposed to high magnetic field shocks was analyzed. Offset sources have been analyzed. It is also emphasized in this study that the amplitude of the excitation signal can be used to improve offset performance [28].

1.3.3 Fluxgate magnetometers designed for use in space missions

The articles in this chapter contain research on spacecraft and fluxgate magnetometers used in satellites to study the magnetic activity of the Earth or other planets. In addition to the functionality of the fluxgate magnetometers used in space applications, there are some requirements that must be fulfilled for compatibility with space conditions. These are volumetric compactness, low mass, low power consumption, temperature variation and high radiation compatibility. A lot of research has been done on these issues and some of them have been presented in this thesis.

In 2006 a thesis on the design of miniaturize fluxgate magnetometer was also published. In this thesis, a digital and miniaturized fluxgate magnetometer design is targeted for use in the ASTRID-2 satellite. This design has been implemented with a digital circuit that is designed with VHDL code on FPGA instead of three layer circuit

structure. As a result, 120x85 mm pcb was made and no new technique or analysis was presented. A small light weight magnetometer design for space applications [29].

In 2007, an article on miniaturize fluxgate magnetometer design was published for space applications. Digital flexibility and easy configurability put digital designs first. The drive signal is digitally generated in FPGA and the sense signal from ADC is also evaluated in the circuit designed on the FPGA. In this design, a sizing of 20x20x20 mm and a power consumption of 330 mW is achieved with a very miniature result of 101 g. In 2014, a magnetometer integrated as an ASIC was designed for magnetospheric studies. The magnetometer designed with this chip is at a noise level of $8\,pT\,/\,\sqrt{Hz}$ with a power consumption of 450 mW with a weight of 76g. 24 bit ADC is used. It has been a successful application because space and power are important in space applications [30].

To make a radiation-hardened FGM, the circuit modules that will be most affected from the radiation should be detected. In a publication published in 2013, the sensor output signal filter and the analog integrator circuit were removed from the magnetometer electronic circuit [31]. Compensation circuit is implemented as full digital and DAC is used. So when using radiation-hardened elements, we need to shape the design accordingly. For example, the fluxgate magnetometer used in the Göktürk field is full analog and the radiation safety is achieved by taking a fluxgate magnetometer into a radiation-hardened box. But if a digital design is used, using radiation-shielded electronic components is more reasonable for both weight and diminution of the magnetometer's volume.

In 2014, an article published by TÜBİTAK UME magnetic laboratory has been studied on optimum diameter information that fluxgate sensors can be used in space applications. For this purpose, 3 different diameter ring core fluxgate sensors have been investigated and analyzed for noise and sensitivity. The result is that the 20 mm diameter sensor performs better than both the 12 mm and 15 mm sensors in terms of noise and sensitivity [32].

Fluxgate magnetometers have been used in many space missions over the past few years. Some academic publications on magnetometers used in these missions are also

available in the literature. One of these is the THEMIS project [33], which was initiated to study the earth's magnetosphere. In this project, dozens of magnetic field measurement stations have been installed on the earth and satellites co-operating with these stations have been thrown away. In this project, 800 mW power consuming digital FGMs with $10\ pT\ /\ \sqrt{Hz}$ noise performance are used to detect magnetic fields up to 64 Hz. These magnetometers are implemented digitally on the FPGA, with the exception of the output preamplifier circuit of the sensor. FGMs used in this task can measure at ±25000 nT. To avoid being affected by environmental noise, the magnetometers on the satellites are placed on the tip of the long pylons (4-8 m) called boom. Thus, it was tried to keep away from the magnetic noise caused by the satellite. Besides investigating the Earth's magnetic field, fluxgate magnetometers are also designed to investigate the magnetic activity of other planets.

One of these missions is the BepiCOLOMBO named spacecraft that was sent to the Mercury planet by the ESA. The FGM used in this vehicle has a power consumption of +2000 nT measurement range of $7-9\ \ pT\ /\ \sqrt{Hz}$ noise and 2.17 W. In this mission, the sensor driver frequency of the magnetometer used is 11 kHz. A 20 bit delta sigma ADC is specially designed and digitized by this component so that magnetometer with 4 pT resolution can be so sensitive [34]. In 2005, the CASSINI named spacecraft was sent to the Saturn planet and its satellite TITAN to investigate their magnetic field properties. The driving frequency of the magnetometer used in this vehicle was chosen as 15.6 kHz square wave. Noise is measured at $5\ pT\ /\ \sqrt{Hz}$ using a 14-bit ADC, so the sensitivity is around 5.4 nT. Total weight is 440 g. The measurement range is designed to be very wide ±44000nT [35]. Other space missions used by Fluxgate magnetometers include MAGSAT, Voyager and Rosetta.

1.3.4 Fluxgate magnetometers designed for use in different disciplines

The use of FGMs has diversified and spread over the years. The fluxgate magnetometers are designed with many different perspectives, from current measurement to NDT, UXO survey, attitude control. These investigations are explained and evaluated under this heading.

Fluxgate magnetometer is a solution for magnetic field measurement in different disciplines. One of these applications is a magnetic gradiometer. Simply a gradiometer is designed with two sensors positioned at a certain distance from each other and is used to determine the gradient of the value to be measured. For this purpose, a gradiometer was designed using two ring core fluxgate sensors to observe the change of magnetic field in the space environment. As a result of this work, a structure that is 3 times less noisy was obtained. A circuit based on digital, FPGA has been implemented as an electronic circuit [36].

Another use of FGMs is the current measurement bias. Current measurements using both fluxgate sensors, both DC and AC, with a 0.7% error in the 0-30 kHz frequency band with a current between 0-20 A were implemented using fluxgate sensors [37]. Furthermore, in a publication published in 2015, ASIC fluxgate current sensors designed for contactless current measurement in high power applications are introduced. For this purpose, an integrated DRV425 code is also available on the market [38].

FGMs are also used in underground surveys. It is important that this area does not drift the signal at high temperatures and that the lock-in amplifier can work stably. A published article in 2015 shows that a fluxgate magnetometer with a frame of "Macor" and sensing coil can operate in a temperature environment of 250 ° C. Thermal drift can be reduced by applications to the lock-in amplifier and driver signals, but the important thing is the material from which the sensor is made [39].

In 2017, the fluxgate magnetometer was designed with the purpose of detecting low-frequency oscillatory movements of earthquakes, large rotating machines and engineering structures, and high angular accuracy was achieved. In this application, a magnetometer is connected with the help of a long rod to determine the oscillation motion and the oscillations up to 64 Hz have been successfully detected [40].

Another area where FGMs are being used as a solution is the detection of unexploded ordnance. Unexploded ordnance under water or on land is a major hazard. High performance was achieved in the detection of undersea UXO where FGMs were used in a series [41].

CHAPTER 2

FLUXGATE SENSOR THEORY AND IMPLEMENTATION

This section describes the parts of ring core Fluxgate sensors and their operating mechanisms. In addition, information about the ring core sensor used in the study made within the scope of the thesis is given.

2.1 Design of Excitation Coil

Among the Fluxgate Sensors, the most common type of sensor used in magnetometer applications is ring core sensors. A ring core fluxgate sensor basically consists of two parts. The toroid excitation bobbin which gives the name of the ring core sensor and the rectangular pick-up coil. The excitation coil is designed as a toroid in Figure 2.1 and the excitation core is made of soft magnetic material.

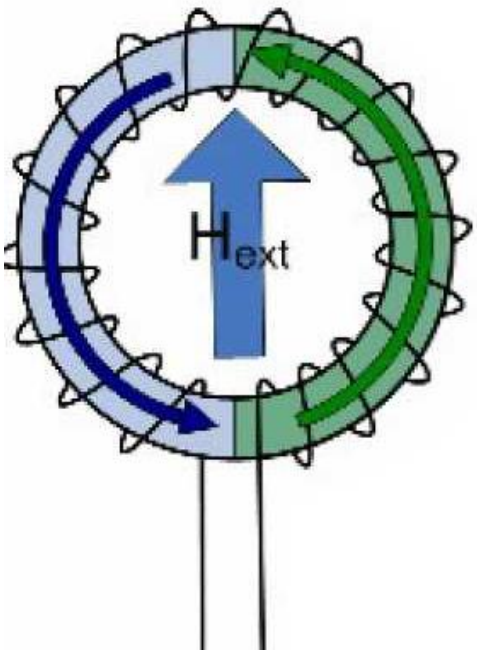


Figure 2.1 Ring core Fluxgate sensor excitation coil [9]

The most critical element for magnetometers to work properly is magnetic core material in strip form manufactured from soft magnetic material. In this thesis, Metglas 2714A Cobalt Based Alloy material was used in the design of the magnetometer.



Figure 2.2 A sample of Metglas material [42]

This material is wrapped 6 times around the hoop made of PEEK material and the ring core is designed. The thickness of this magnetic stripe has been chosen to be at least 15mm in order to contribute to low noise performance by reducing eddy currents to low power consumption. The drive toroid coil was obtained by wrapping 126 turns around the core with 300 µm copper wire. Another characteristic of the core material is that the used strip ~ 0.57 T is saturating the magnetic field and the magnetic permeability is in the order of 10^5. Metglas material used is made of magnetic alloys (iron, nickel, cobalt boron, silicon) containing magnetic domeins. This material is obtained in strip form by pouring on a rotating cold wheel while molten at high temperature. Thus this special material is uncrystallized. Uncrystallized metal alloy has an amorphous molecule structure such as glass, and the internal unit domeins are formed in a minimum size. Thus amorphous glassy metal strip core material is obtained. The fact that the magnetic domains are so small caused it to be affected even from very weak magnetic fields, and so it is called soft magnetic material. It is thus possible for magnetometers to detect very weak magnetic fields. The characteristic B-H curves of various conditions of the material used in the fluxgate sensor design are shown below.

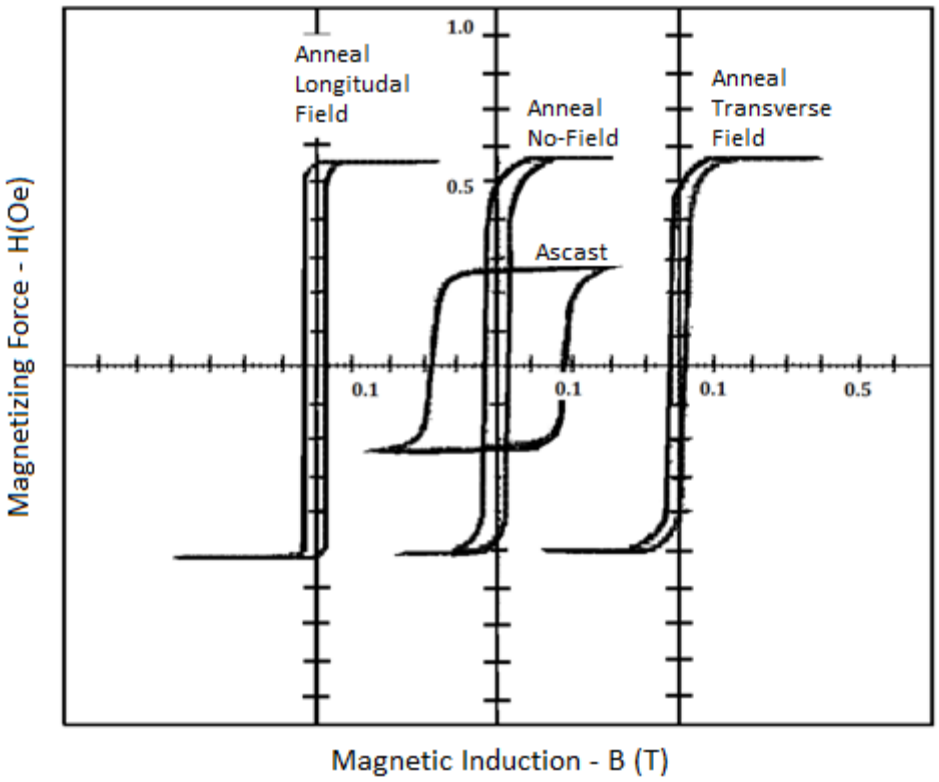


Figure 2.3 Hysteresis loops of Metglas 2714A material [43]

As shown in Figure 2.3, the Metglas 2714A B-H characteristic, which is a very low coercive field value model, is modeled by the following equation.

$$B(t) = 3 * H(t) - H(t)^3 \quad (2.1)$$

$$H(t) = H_{ext} + h * sin\omega t \quad (2.2)$$

H_{ext} is the measured external magnetic field, $h * sin\omega t$ is the signal applied to the drive coil.

2.2 Design of Pick-Up Coil

Pick-up coil is designed from PEEK material, so that the excitation coil can be inserted into the pick-up coil. This structure was wrapped with 200 µm copper wire in 575 turns. Technical drawing and winding diagrams for the pick-up coil are shown in the following figures.

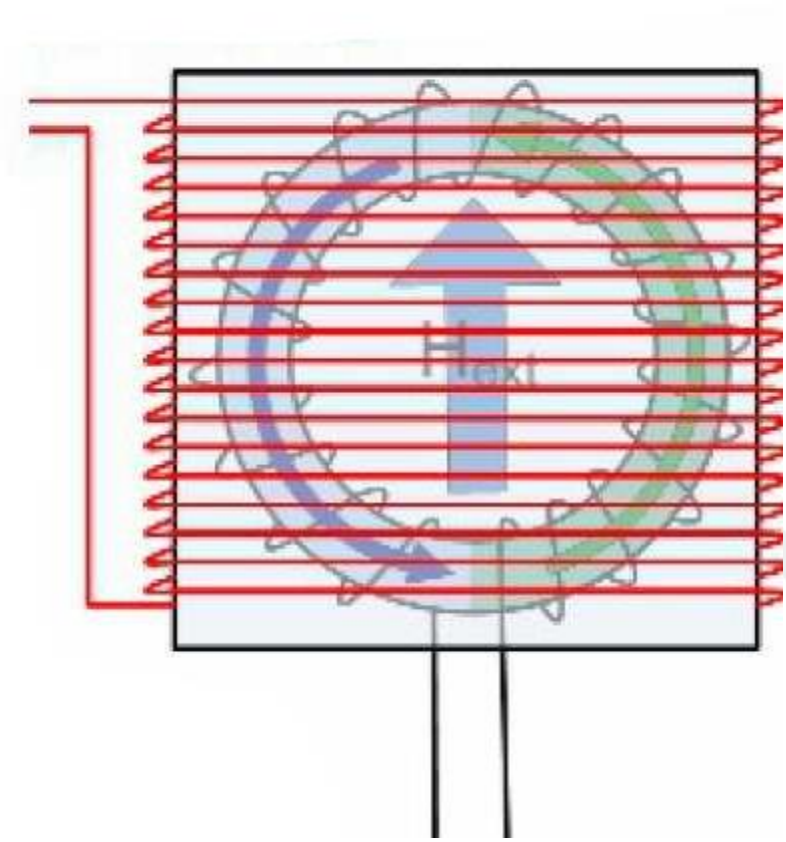


Figure 2.4 Ring core Fluxgate sensor pick up coil [9]

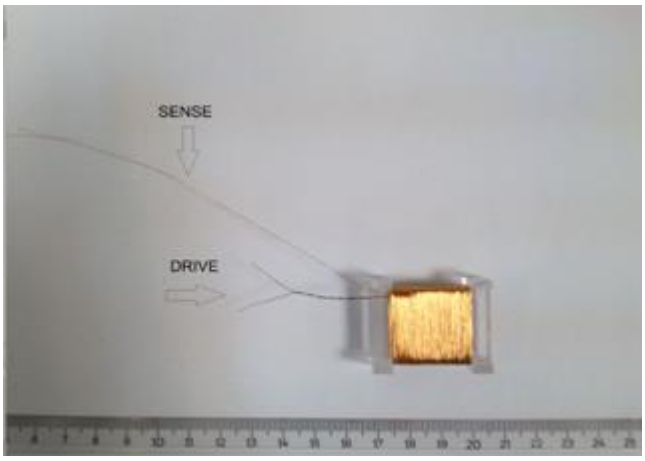


Figure 2.5 Winding of pick-up coil

2.3 Working Principles of Ring Core Fluxgate Sensor

Ring core sensors are excited by the signal applied to the excitation coils and the magnetic field is measured by analyzing the harmonics generated in the pick-up coil. This can be expressed mathematically by modeling the B-H curve of the core material.

$$B(t) = 3 * H(t) - H(t)^3 \quad (2.1)$$

$$H(t) = H_{ext} + h * sin\omega t \quad (2.2)$$

If the expression $H(t) = H_{ext} + h * sin\omega t$ is written instead of H (t) in (2.1), the following mathematical equation is obtained.

$$B(t) = H_{ext}\left(3 - {H_{ext}}^2 - 1.5h^2\right) + 3h\left(1 - {H_{ext}}^2 - 0.25h^2\right)\sin(\omega t) + 1.5H_{ext}h^2\cos(2\omega t) + 0.25{H_{ext}}^3\sin(3\omega t) \quad (2.3)$$

Resulting field is in (2.4).

$$B(t) = \cdots + 1.5H_{ext}h^2\cos(2\omega t) + \cdots \quad (2.4)$$

The sum of the signals obtained in the pick-up coil is found by (2.3). In this equation, the mathematical expression which is linearly related to the external magnetic field is found (2.4) If the mixed signals from the pick-up signal are cleaned with a filter that passes the 2f band, the external magnetic field can be measured. The expression in (2.4) pick-up signal has twice the drive signal frequency. Therefore, the output signal of the fluxgate sensors is a signal with a frequency of 2f.

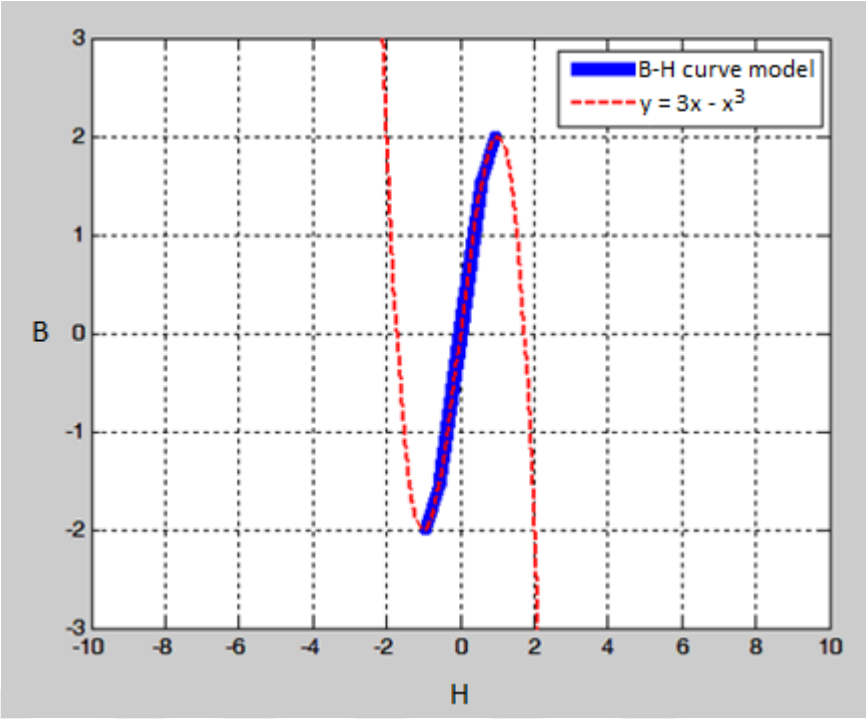


Figure 2.6 Mathematical Model of Metglas 2714A's B-H curve

All this information can be interpreted in the light of the driver and pick-up output signals of the ring core fluxgate sensor. In this context, fluxgate ring core excitation and pick-up signal can be seen in the figure below.

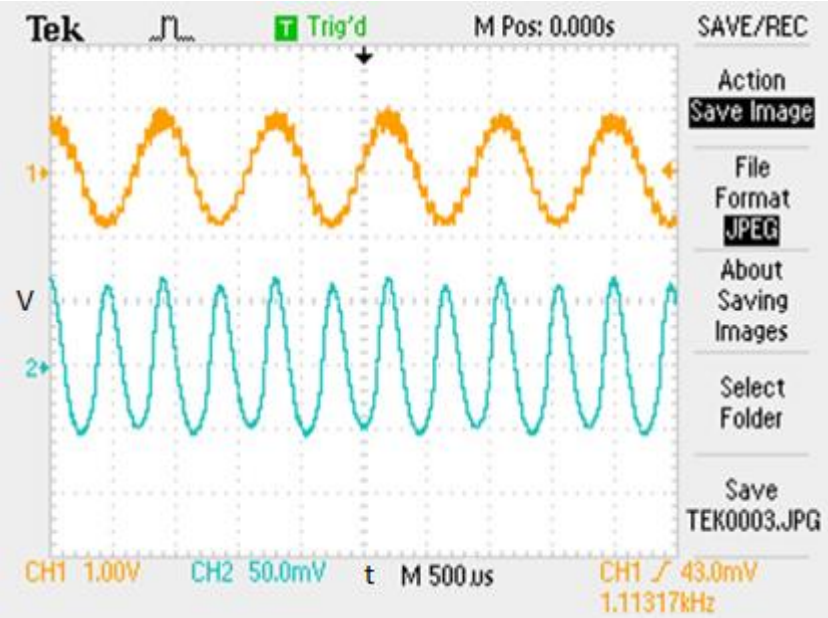


Figure 2.7 Excitation (orange) and Pick-up (blue) signal of Fluxgate Sensor

The excitation and pick-up signals seen above are fluxgate sensor signals that are designed within the scope of this master thesis. After this phase, the design of the driver and sensing electronics and the work on the lock-in amplifier technique will be presented.

CHAPTER 3

LOCK-IN AMPLIFIER DESIGN

In this section, a lock-in amplifier study, a mathematical lock-in amplifier model, and a digital lock-in amplifier algorithm designed by this method are explained.

3.1 Introduction to Lock-In Amplifier

The lock-in amplifier is basically a very high and narrow band amplifier with Q value. Even in an extremely noisy environment, if the carrier frequency is known, it is easy to get a weak signal. It does not raise unnecessary noises because it has a narrow amplifier band. This process is performed by multiplying this signal by a reference signal having the same frequency as the carrier of the signal to be amplified. Even if conventional lock-in amplifiers use analog frequency multipliers and RC filters for demodulation, state-of-the-art devices perform both stages through fast digital signal processing on the FPGA. Generally, sinus and cosine demodulation are performed simultaneously, which is called dual-phase demodulation. This allows the acquisition of in-phase and quadratic phase components, which can then be transferred to polar coordinates, i.e., amplitude and phase, so that the result can be processed as a real and imaginary part of a complex number.

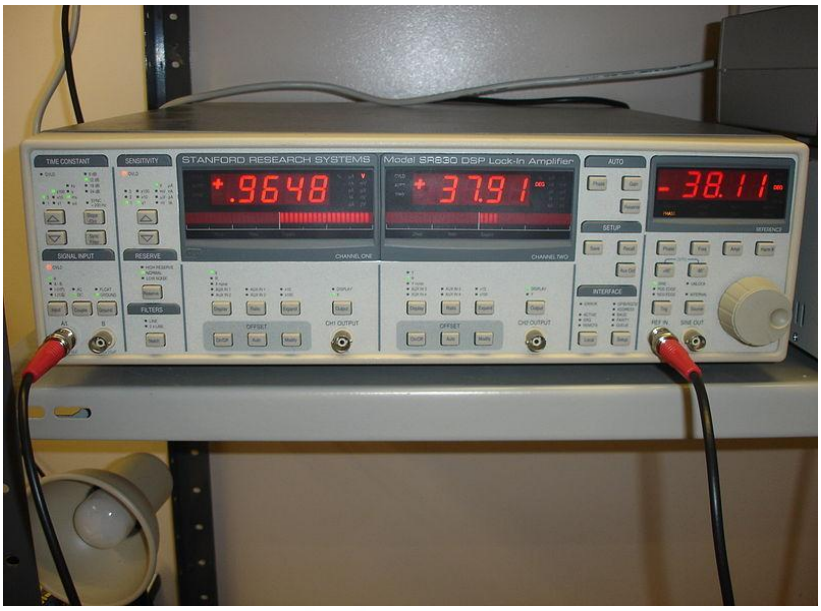


Figure 3.1 A standard lock-in amplifier for laboratory use [44]

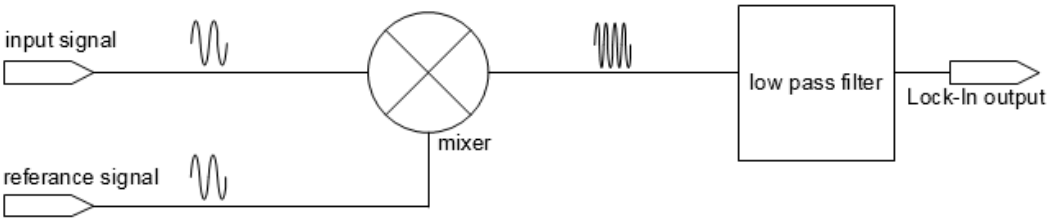


Figure 3.2 Single-phase basic lock-in amplifier circuit diagram

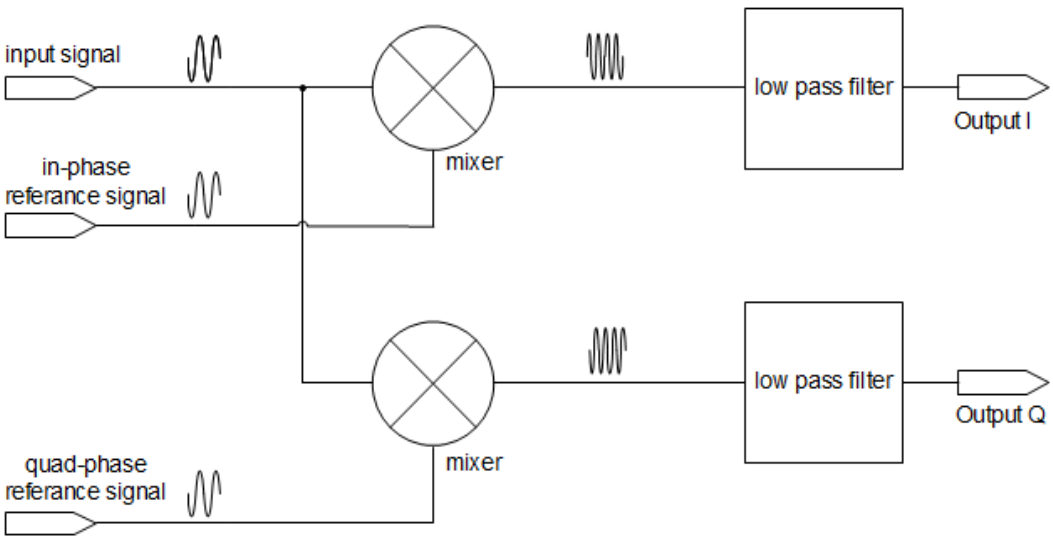


Figure 3.3 Basic two-phase lock-in amplifier circuit diagram

3.2 Fundamentals of Lock-In Amplifiers

The amplifier designs conceptually have an amplifier gain and amplification bandwidth. For example, a signal with amplitude 10 nV and frequency 40 kHz is wanted to be amplified 100 times. When an amplifier with a boost band of 200kHz is used, this amplifier amplifies the 40kHz signal while the other signals in the 200kHz band are amplified, especially when the noise is also amplified. In an environment with 5 nV(Hz)$^{1/2}$ of environmental noise, a 200 kHz bandwidth and a Q = 1 amplifier will produce 2.2 mV noise at the output. If this band was 40 kHz and the Q value was 100, this time the output noise would be 100 μV

$$100nV * \sin(40kHz) * 1000 = 100\mu V * \sin(40kHz) \quad (3.1)$$

$$5nV * 1000 * \sqrt{200kHz} = 2.2mV \quad (3.2)$$

$$5nV * 1000 * \sqrt{\frac{40kHz}{Q}} = 100\mu V \quad (3.3)$$

If the gain constant is 1000, and signal amplitude $100\ nV$. In (3.2) of, the desired signal to be amplified is lost in the noise signal. In (3.3) desired signal to be amplified is equal the noise signal. At this stage very narrowband (very high Q) amplifiers are required in order to be able to amplify very low amplitude signals without being affected by ambient noise. In the Phase Sensitive Detection technique, the amplifier Q value goes up to 10,000 and very narrow band amplification can be performed. PSD is a technique used in the demodulation process and processes the product of the periodic signals. In this technique, the input signal to be amplified is multiplied by a reference signal having the same frequency.

$$V_{out} = V_{in} * V_{ref}(\cos(2\omega t) * cos\theta - \cos(\omega t) * \sin(\omega t) * sin\theta) \quad (3.4)$$

$$= \frac{(V_{in} * V_{ref})}{2} * (\cos\theta + \cos(2\omega)\, t * \cos\theta - \sin(2\omega t) * \sin\theta) \quad (3.5)$$

$$= \frac{(V_{in} * V_{ref})}{2} * (\cos\theta) + \frac{(V_{in} * V_{ref})}{2} * \cos(2\omega t + \theta) \quad (3.6)$$

Not: (θ = phase difference between input signal and reference signal)

The DC component of the resulting 2ωt carrier frequency signal carries information about the magnitude and phase of the signal to be amplified. If this DC component is filtered with LPF, the basic phase and amplitude information for the signal to be amplified is obtained in a combined form. The following figure is a schematic representation of the PSD theory described by the above equations.

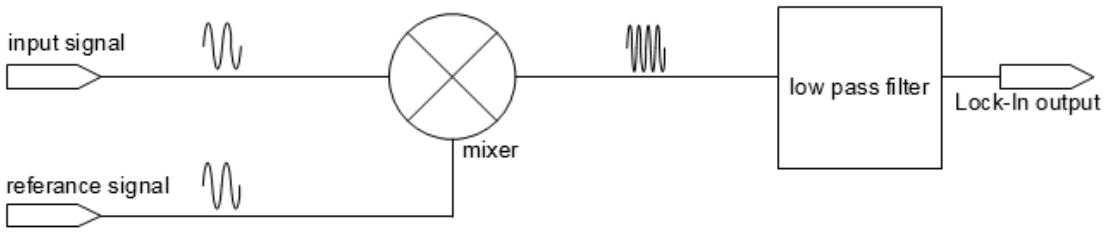


Figure 3.4 Single-phase PSD, lock-in amplifier scheme

3.3 Analog Lock-In Amplifier Design

For ease of implementation in Fluxgate magnetometer design, analog lock-in amplifier design can be used in some cases. In such a case, it is necessary to prepare this process before the sensor output signal is multiplied. The signal going from the sensor output to the lock-in amplifier passes through the preamplifier first. This is usually the instrumentation amplifier element to which the sensor outputs are connected. The pick-up signal is then passed through an AAF or BPF that passes the 2f frequency and is ready for multiplication. This signal arriving at the multiplication operation section is multiplied by a reference signal having a frequency of 2f, whose phase and amplitude are known. As a result of this multiplication, a signal having a frequency of 4f and a DC component is generated as described above. This DC component is a phase and amplitude dependent value of the sensor output signal and is filtered with the aid of a low-pass filter as the final output of the lock-in amplifier circuit. This low-pass filter should be designed with a cut-off frequency lower than 1 Hz for the DC component cleaner. If both the phase and the amplitude of the fluxgate sensor output signal are to be calculated separately, then the dual-phase lock-in amplifier architecture should be preferred. In this structure, the fluxgate sensor output signal is multiplied by two reference signals of zero degree phase and 90 degree phase with 2f frequency. These

two product results will be passed through two separate LPFs, resulting in two separate DC results. These results are represented by Q because the results are multiplied by the in-phase (0 degree phase) reference signal and the other is multiplied by the quadrative-phase (90 degree phase) reference signal. From these two fixed numbers, the phase and amplitude of the input signal can be calculated according to the following formulas.

$$Magnitude = \sqrt{(Q^2 + I^2)} \quad (3.7)$$

$$Phase = tan^{-1}(Q/I) \quad (3.8)$$

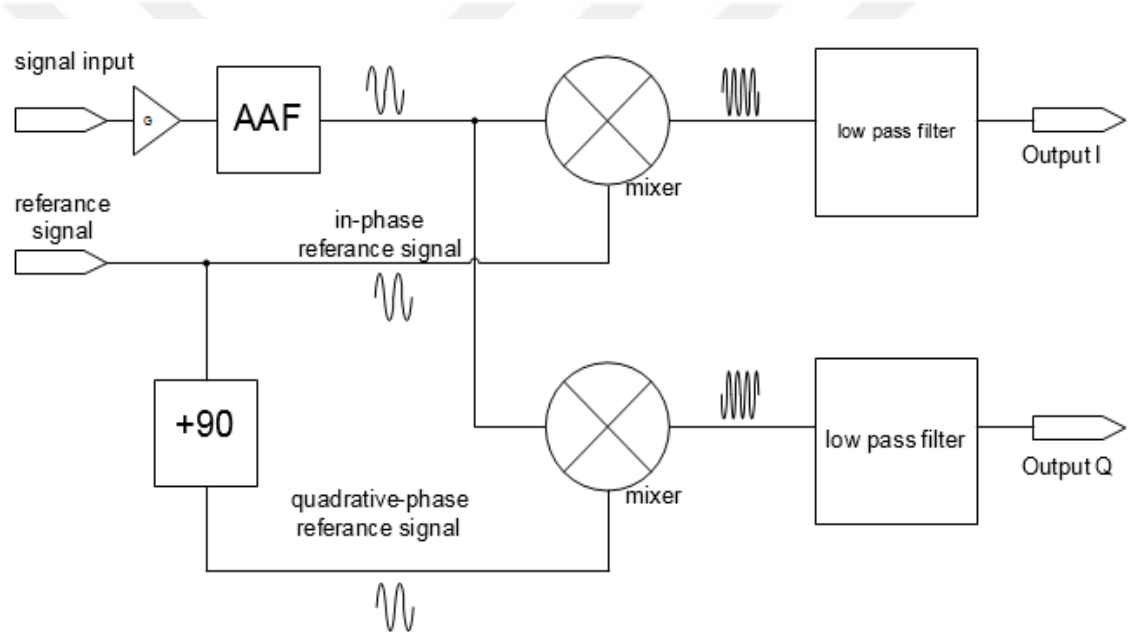


Figure 3.5 Analog Fluxgate magnetometer block diagram

3.4 Digital Lock-In Amplifier

Digital Lock-In amplifier applications are usually implemented on DSP elements. In these designs, the ADC resolution is the width of the amplification band. In systems with ADC, bandwidth is limited because it depends on ADC speed. Because of this, digital lock-in amplifier structures are behind analog lock-in amplifiers in terms of quenching band. In DLIA, the reference signal is internally generated by a DAC or PWM source. From this point of view, problems of adjusting the phase and amplitude of the

reference signal encountered in ALIA are minimized in the digital design. In addition, 90 degree phase shifting of the quadratic reference signal can be performed with much higher sharpness. The internally generated in-phase and quadrative phase reference signals are multiplied by the input signal using any DSP element or, in particular, dsPIC products from Microchip. It has been digital with the digital input signal (pick-up) through the ADC

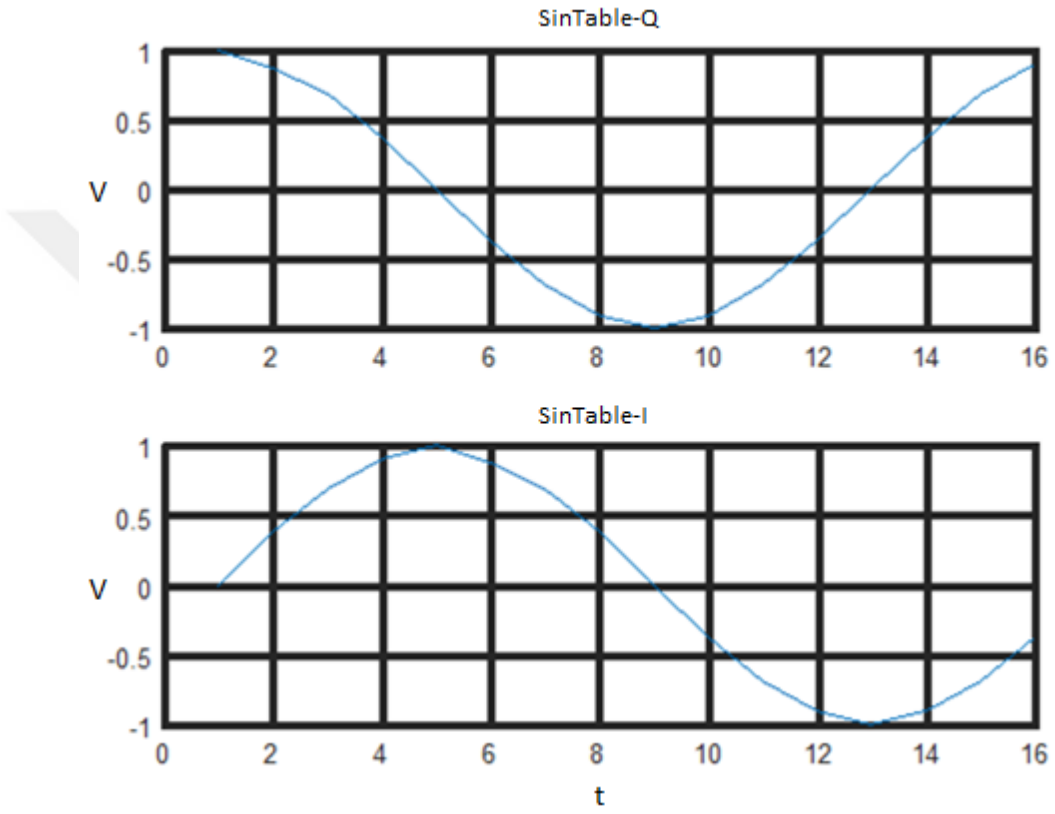


Figure 3.6 0 and 90 degree phase, in phase and quadrative phase reference signals

A processor with DMA module is used from the dsPIC series microcontrollers so that the microcontrollers can be busy while this multiplication operation is being performed. With the help of this DMA modul, two 16-bit segmented reference and input signals are multiplied to form two separate product result sequences. After this step, the product results stored in memory are passed through low pass filters to obtain DC values. For this operation, FIR filters with coefficients are used so that the cut-off frequency is very close to zero.

In this study, DsPIC33e series processor was used and the C code to run was written. Previously this code was simulated in a MATLAB environment and C and MATLAB results were compared. The following figures of C and MATLAB code output are shown.

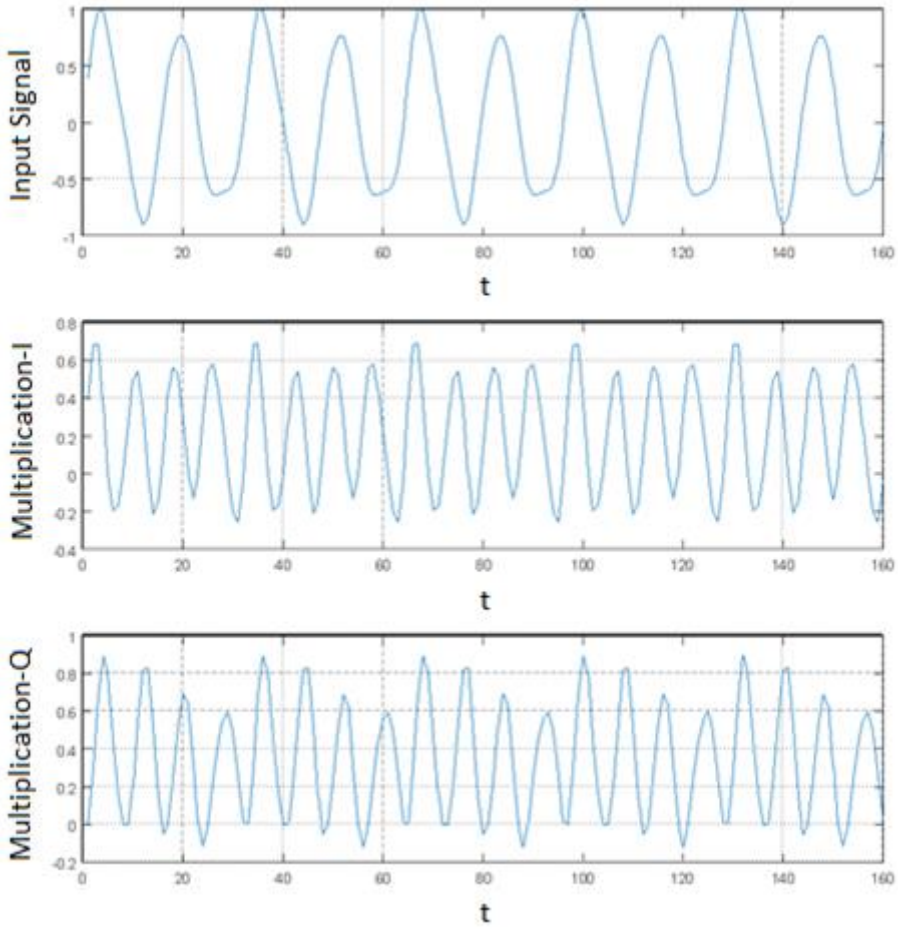


Figure 3.7 Multiplication with input signal and reference signal

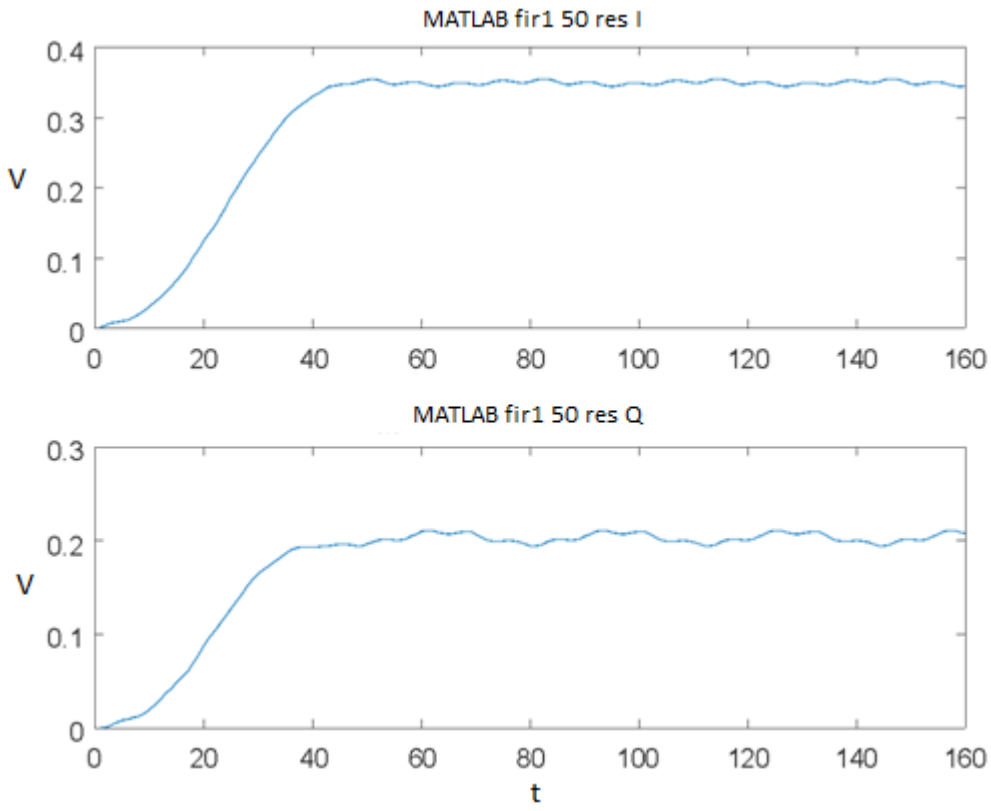


Figure 3.8 FIR filtering results with π / 3 phase difference

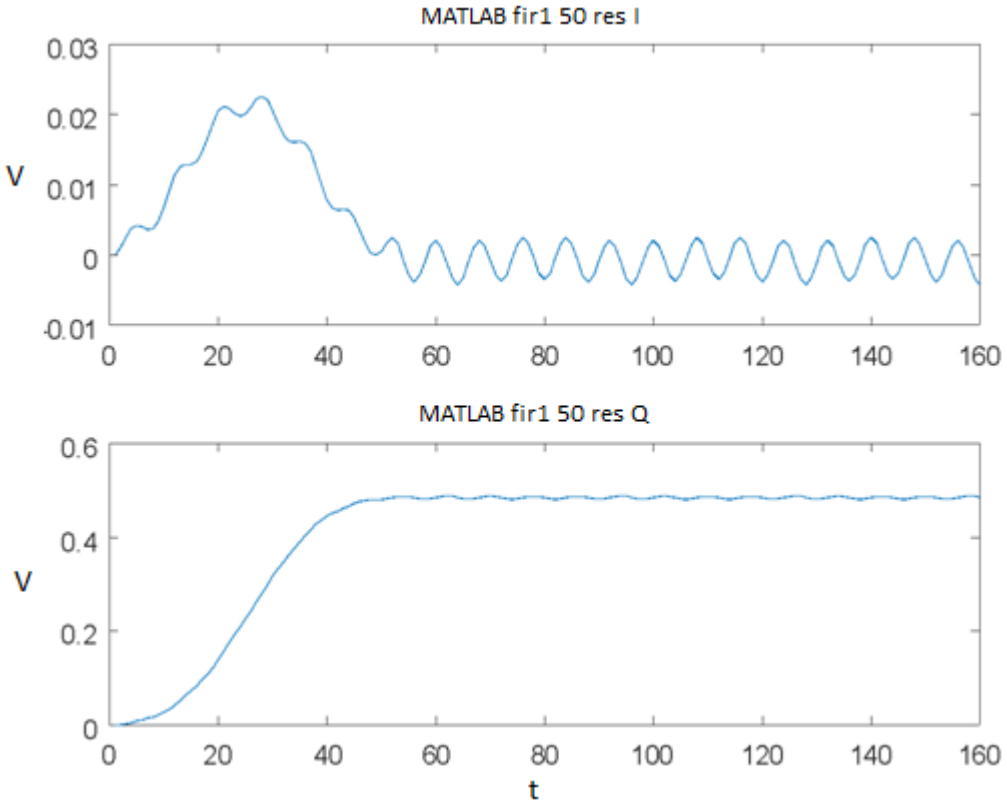


Figure 3.9 Two-time filtering FIR filter outputs with 0 degree phase difference

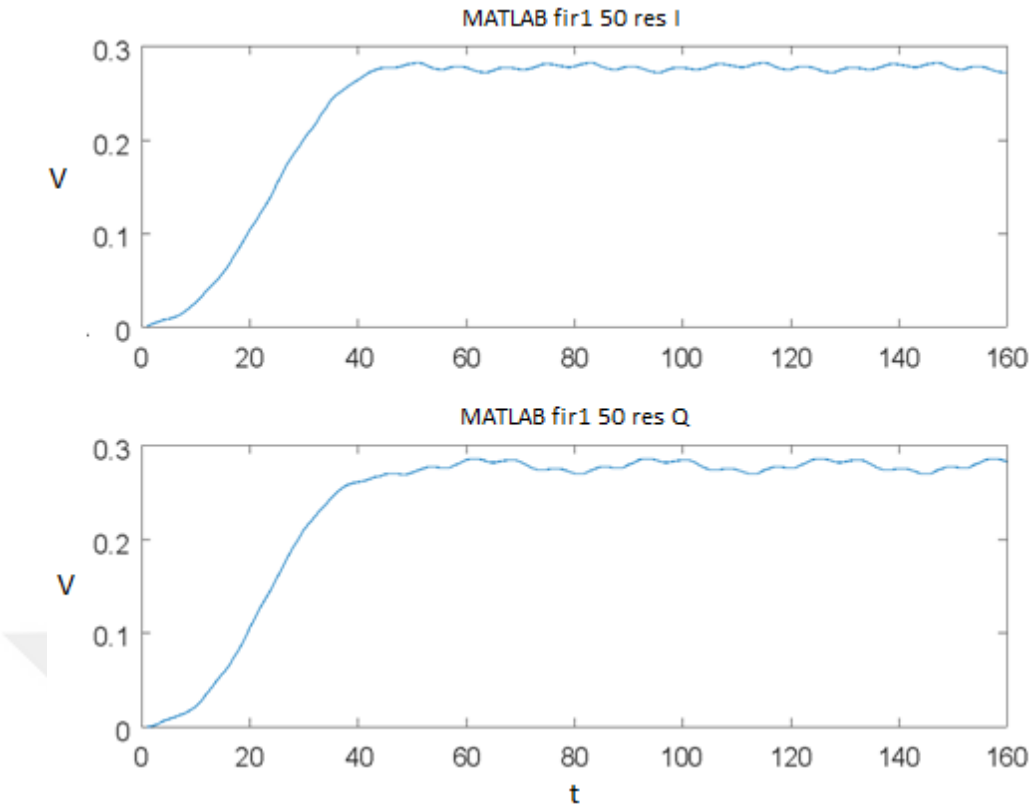


Figure 3.10 two-stage filter outlet with π / 4 phase difference

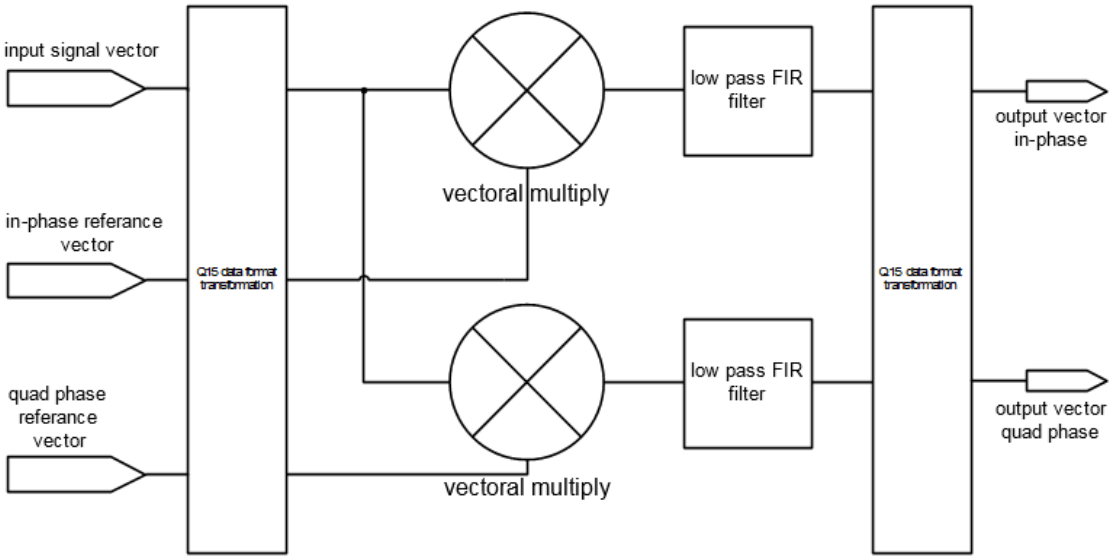


Figure 3.11 DLIA digital circuit schematic

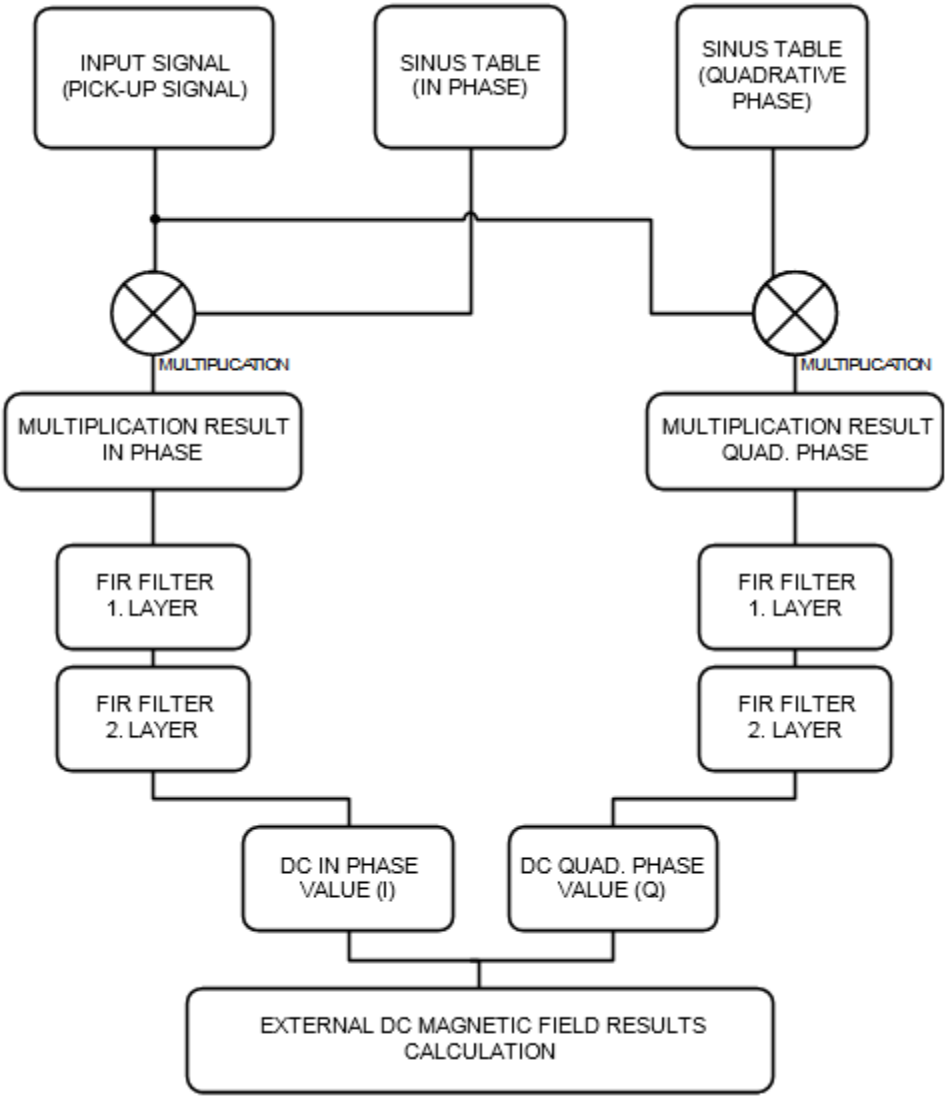


Figure 3.12 DLIA algorithm flow chart in MATLAB and C++

As shown in Figure 3.11 and 3.12, DLIA and C ++ environment are converted to Q15 data format in order to process with filter coefficients. With this conversion, the FIR filter coefficients that take values between 0 and 1 can be written as 16-bit numbers. With this conversion, the desired filtering is achieved. This output can be observed from the filter result graphs.

It can be observed how the in-phase and quad phase results are related to the phase difference between the input signal and the reference signals when the filtering results of Figures 3.8, 3.9 and 3.10 are examined. When the phase difference is 0 degree, the in-phase FIR filter result average is 0 quad phase FIR filter result maximum value. When the phase is $\pi/4$, both FIR filter results are equal.

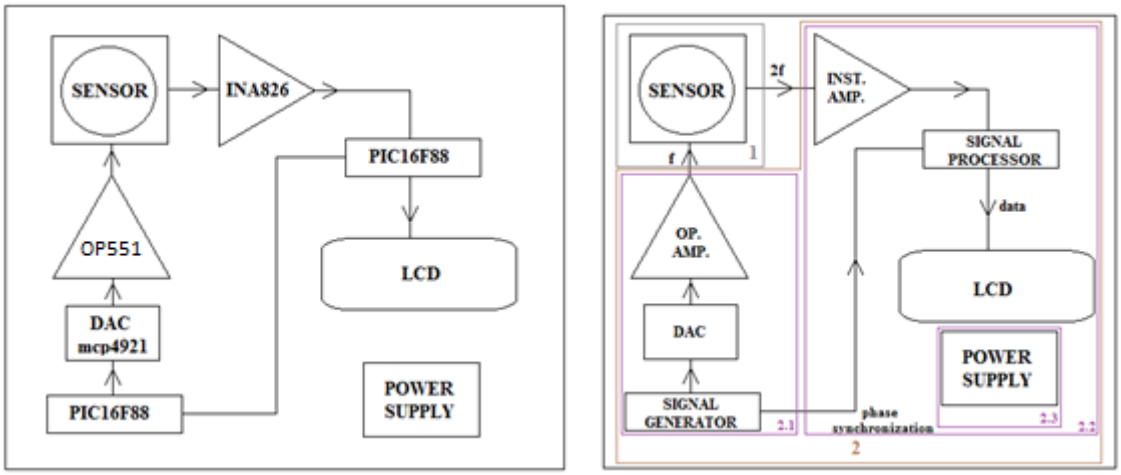
CHAPTER 4

FLUXGATE MAGNETOMETER DESIGN

This section describes a digital fluxgate magnetometer designed in the scope of this thesis. Firstly, we describe the studies and conclusions regarding the design of the sensor driver circuit, the generation of the output of the sensor and then the processing of the pick-up signal.

4.1 General Design Approach of Fluxgate Magnetometer

The Fluxgate magnetometer has two main blocks that is given in Figure 4.1 First block is the fluxgate sensor, which is composed of two coils, pickup coil and excitation coil. Pick-up coil (sense coil) was wound around a 3D frame with a wire diameter of 300 µm. The second coil was used as an excitation coil (drive coil), which is located inside of the pick-up coil frame. It was wound around a circular core as a toroidal and its diameter is 200 µm. The other main block is the electronic circuit of the magnetometer. This electronic circuit consists of two microprocessors. PIC16F88 processes the second harmonic signal of fluxgate pick-up sensor so it calculates DC magnetic field magnitude value and its direction. PIC16F688 was used as a driver signal generator and MCP4921 was used as a DAC. To present all these data, LM016L, 16x2 LCD was used. To supply enough power for all magnetometer system a SMPS which supplies ±10V DC was used.



(a) (b)

Figure 4.1 Digital Fluxgate Magnetometer (a) Circuit diagram (b) Main blocks

In this study, the designed digital fluxgate magnetometer electronic circuit consists of two subsections. According to the schematic shown above, these are the pick-up circuit that receives and operates the fluxgate sensor output signal and the fluxgate sensor driver circuit.

4.2 Fluxgate Magnetometer Driver Circuit

In the designed magnetometer, sinusoidal drive signal at frequency of 1.086 kHz and amplitude of $1.31\,V_{RMS}$ was preferred. This signal was generated by an 8-bit microcontroller with PIC12F675 code. It had been converted to an analog signal with the MCP4921 digital analog converter element. This signal was amplified with the OPA551 operational amplifier element before the drive was applied to the driver coil, thus allowing sufficient current to flow. The drive coil was resonated at 1.086 kHz to deliver maximum current to the drive coil. To achieve this, the appropriate value of the capacitor was connected in parallel to the drive coil. The following figure shows the signal applied to the drive coil.

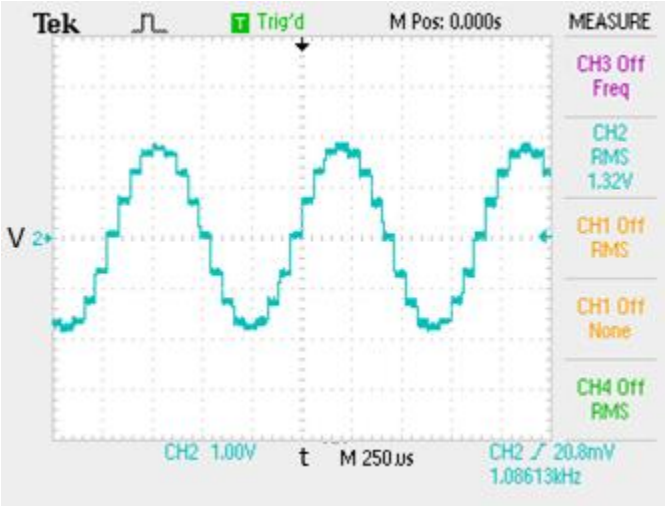


Figure 4.2 Driver signal of Fluxgate sensor

4.3 Fluxgate Magnetometer Pick-Up Circuit

Another part of the designed electronic circuit was the pick-up circuit. This circuit was designed to analyze the pick-up signal generated by the Fluxgate sensor at the output frequency of 2.172 kHz. This circuit basically determines the amplitude value of the output signal as V_{RMS} and the fluxgate sensor's orientation in a fixed plane. For this purpose, the pick-up signal was amplified in the INA826 instrumentation amplifier element and superimposed on the 2.5 V constant offset value. The purpose of doing this was to make sure that the signal from the pre-amplifier did not have a negative voltage value when entering the PIC16F88 microcontroller. Figure 4.3 shows the second harmonic signal versus external DC magnetic field graph. To characterize the sensor, an excitation frequency of 1.086 kHz and excitation voltage of 1.31 V_{RMS} were applied. Excitation frequency was chosen very low due to the limitations in the signal processing circuit. Frequency and amplitude of the excitation signal are the key features in order to find best magnetometer form. Suggested that working frequency around 15 kHz is suitable for an influential sensor application in large scale. However, as seen from Figure 4.3, the second harmonic signal shows good linear dependence between -1.25 and +1.25 Oe. The R-squared coefficient was determined as 0.99998. The slopes of the fitting lines drawn at linear part of the data can be regarded as the

sensitivities of the fluxgate sensor. The sensitivity of ring-core fluxgate was determined as 241 V/T.

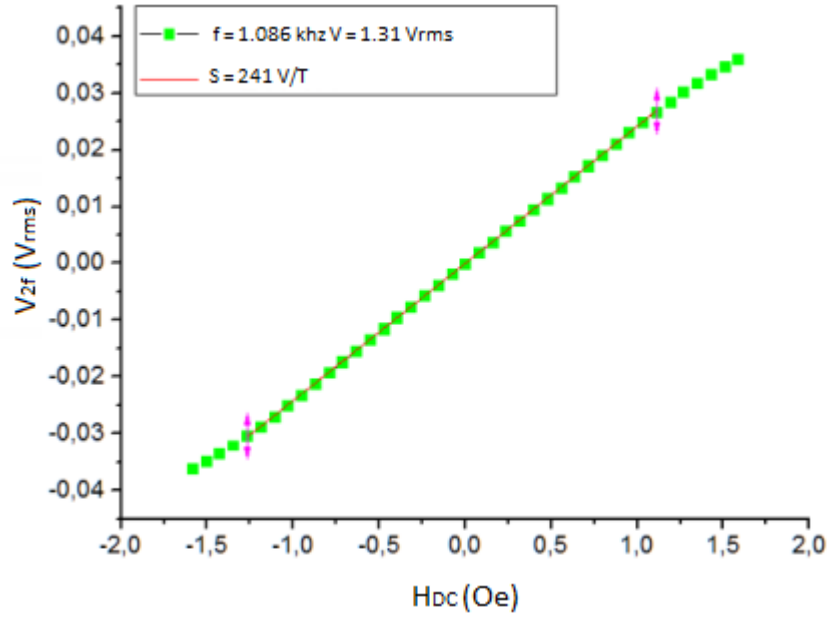


Figure 4.3 Second Harmonic Signals versus External DC Magnetic Field

The pre-amplifier was amplified and the signal with 2.5 V offsets was related to the external DC magnetic field as shown in the above figure. After this step, the PIC16F88 inputs from the microcontroller's ADC pin. The phase and amplitude of the digitized pick-up signal were calculated by the designed algorithm. Amplitude finding was obtained by dividing 20 ADC samples taken for a period into 20 samples. Amplitude value in V_{RMS} was calculated. Phase detection was performed by sensing the behavior of the pick-up signal observed. Here, the PIC12F675 microcontroller, which generates the driver signal, generates a constant pulse signal according to the driver phase. This signal detection was taken as input to the PIC16F88 microcontroller and the phase control was done according to this signal.

According to observations, the output pick-up signal of the sensor rotating on a fixed plane was rotated by 180 degrees and the sinusoidal phase changed 180 degrees. When the fixed phase control signal operator is input, it is checked whether the amplitude of the pick-up signal from the ADC is below the 2.5 V reference. The pick-up signal amplitude measured at the appropriate phase is measured. If the voltage is less than 2.5 V, the calibration result is determined as north/south with the result,

otherwise the opposite direction is determined. The application was made accordingly. Oscilloscope views of these observations are clearly visible in the figures below.

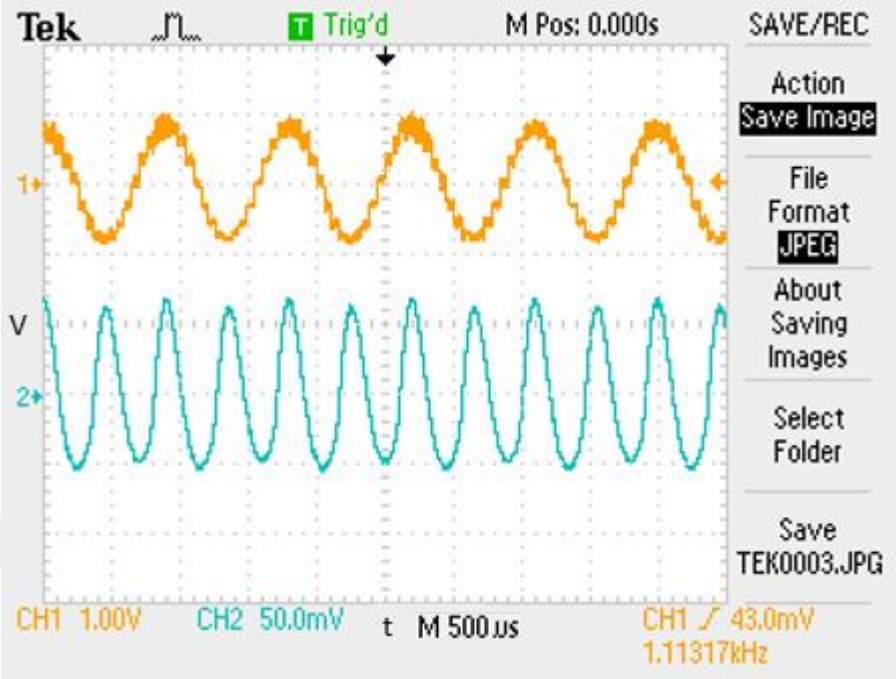


Figure 4.4 Negative value of pick-up signal in zero phase

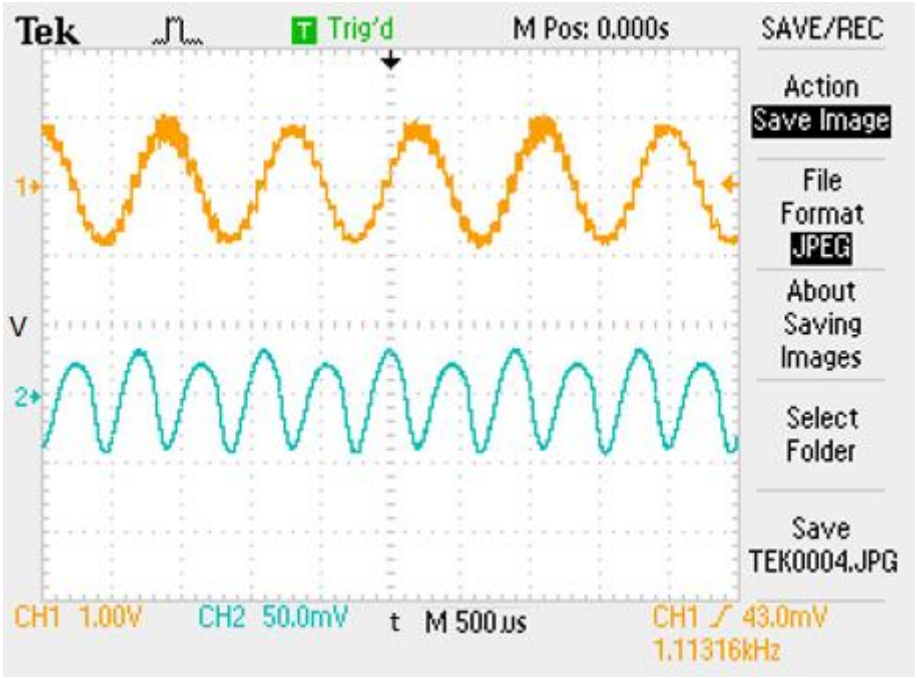


Figure 4.5 Positive value of pick-up signal at zero phase

As a result of the fluxgate Magnetometer design approaches described above, the circuit diagram shown in the following figure has emerged. The digital fluxgate magnetometer is implemented according to this schematic.

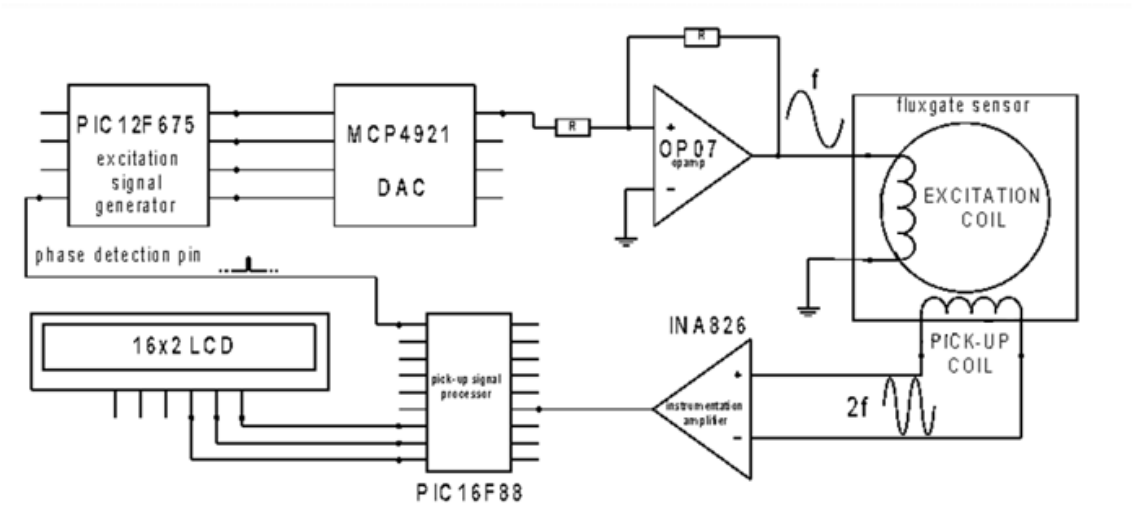


Figure 4.6 Entire Fluxgate magnetometer circuit schematic

This circuit was powered by a ±10 V SMPS source. Electronic circuit and sensor are put in special boxes. The driver and pick-up signal connection between them was provided by coaxial cables. The picture of the whole fluxgate magnetometer system is the same as Figure 4.7.

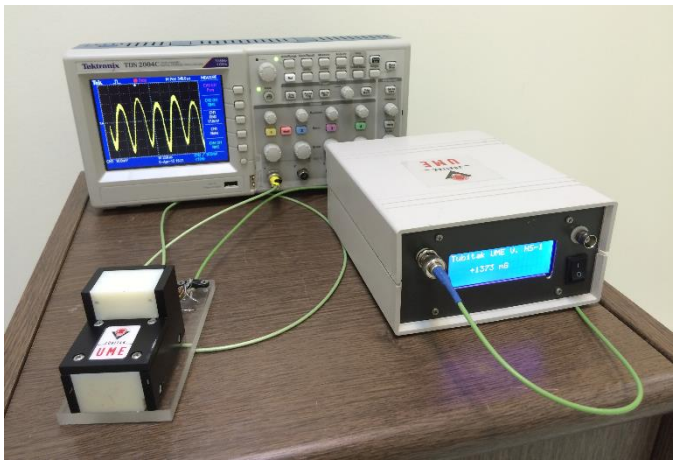


Figure 4.7 The entire system image of the designed Fluxgate Magnetometer

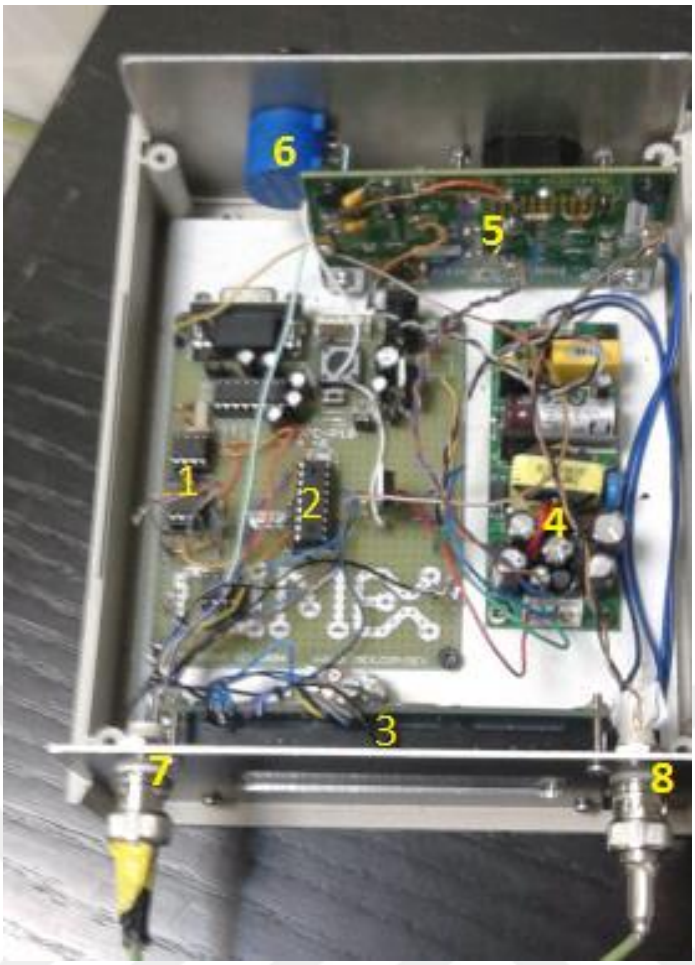


Figure 4.8 Designed Fluxgate magnetometer's circuit connections

The fluxgate magnetometer, designed and capped in the above figure, shows circuit connection and settlement. Figure 4.8 shows the section where the driver signal and phase detection signal are generated in section 1. Microcontroller used in the pick-up circuit is shown in section 2. If it is explained through this image, the signal from driver number 1 goes out from the port indicated by number 7 and the sensor goes to the driver coil. The signal generated by the sensing coil of the sensor also enters the port labeled 8. Hereafter, in order to be compatible with the digital system, the number 5 is entered here, which is then amplified by the INA826 and superimposed on an offset. In section 6, the gain of the pick-up signal is set. The signal from section 5 and 6 comes to the microcontroller element with pick-up signal processing indicated by number 2. The signal is evaluated by the running algorithm here. Values related to the detected DC magnetic field by means of the sensor are presented to the user in the area indicated by the number 3. This is the circuit connections and the workflow of the system.

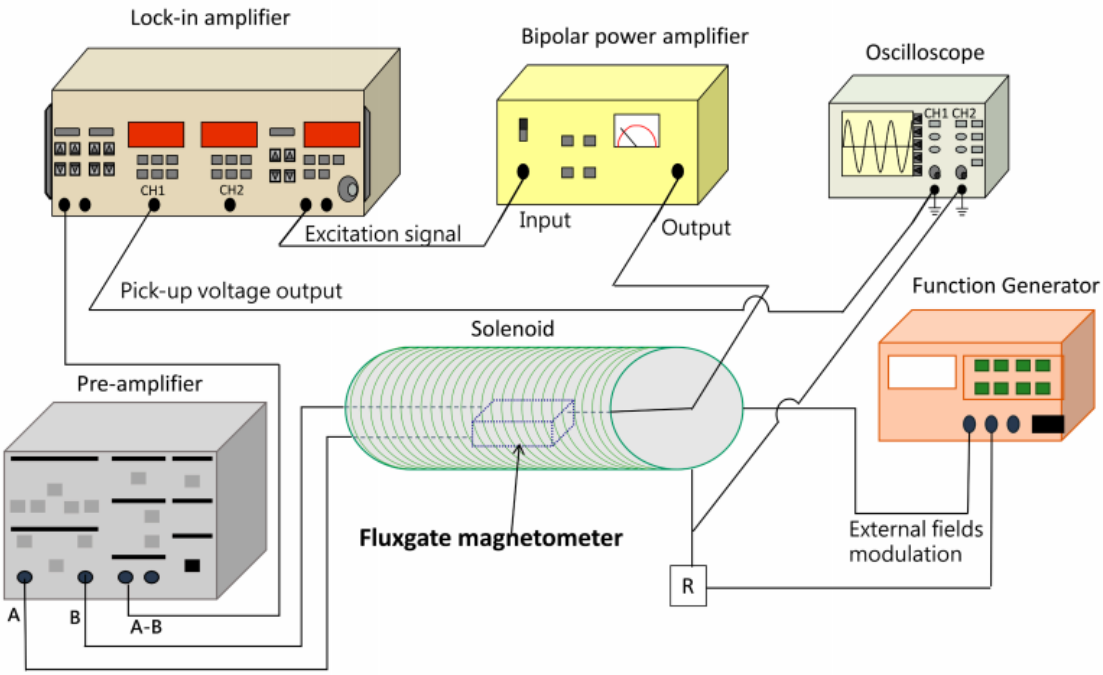


Figure 4.9 Fluxgate magnetometer sensitivity measurement setup

Sensitivity measurements were made after the Fluxgate magnetometer was designed. According to the above figure, the drive signal is applied to the fluxgate magnetometer placed in a helmholtz coil and the output is input to the lock-in ampilfier device. At this time, a linear current was applied to the helholtz coil to simulate the external magnetic field. Thus, all the values between -2 G and + 2 G were scanned and the output signal of the magnetometer was analyzed. The resulting fluxgate magnetometry precision chart is obtained.

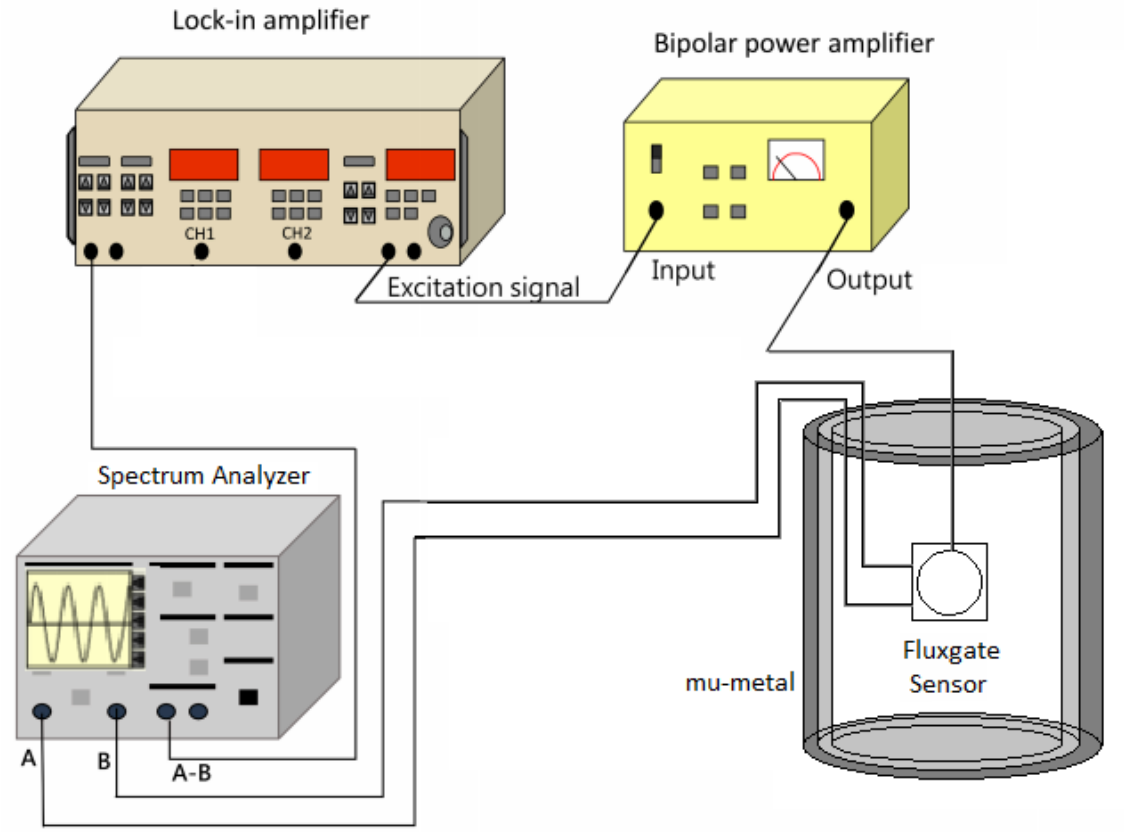


Figure 4.10 Fluxgate magnetometer noise level measurement setup

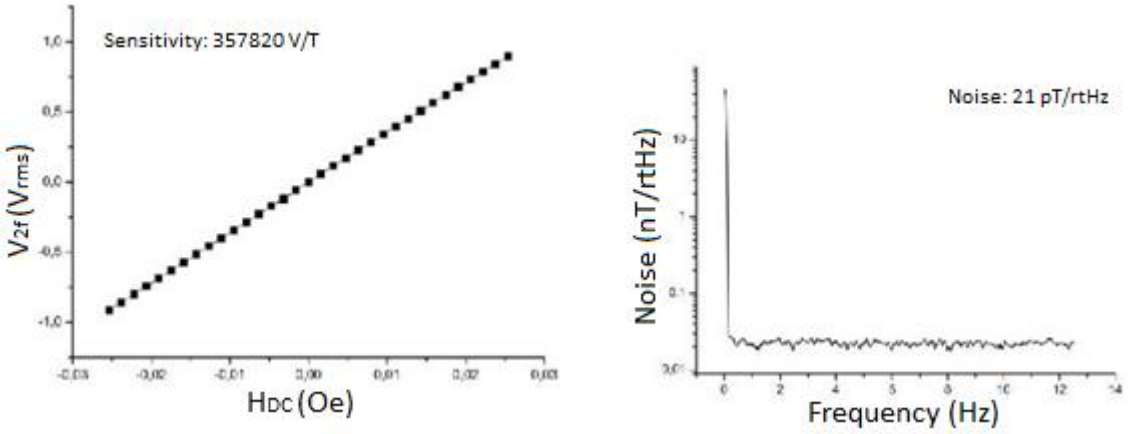
Noise measurements were made after the Fluxgate magnetometer was designed. According to the above figure, a fluxgate magnetometer placed in a mu-metal (magnetic insulating material) is applied drive signals at different frequencies and the sensor output signal spectrum analyzer is entered. As a result, the entire frequency band was scanned and the noise level graph of the designed fluxgate magnetometry was obtained. The average noise was measured as 21pT/ rTHz.

4.4 Application

4.4.1 TUBITAK UME Fluxgate Magnetometer Application

Magnetic sensors can find many different applications such as space application, archeology, medicine, mining, defense. In parallel with the diversity of application areas, sensor selection is also important. For example, if navigation is used, the dynamic range of the sensor should cover the range of 10^9 -$10^4\ T$. On the other hand, it is enough for the sensor to have the ability to measure 10^5 -$10^3\ T$ in order to investigate the regional irregularities in the earth's magnetic field. Although there are many metrologically acceptable and reliability-tested measurement methods in the high magnetic field area ($> 10^5\ T$), the method accepted in the low field area (10^{15} -$10^5\ T$) is quite limited.

The UME Magnetic Measurements Laboratory has developed a Fluxgate Magnetometer that is minimally affected by environmental parameters (temperature, pressure, etc.) capable of measuring DC magnetic field magnitudes from 10^4 Oe to $10^9\ T$ in a magnetometer project initiated in 2010. The sensitivity and noise measurements of the 1st generation UME Fluxgate Magnetometer are shown in Figure As shown in figure (4.9)(a), there is a perfect linear relationship between the DC field to be measured and the sensor output signal, which is of great metrological significance. On the other hand, as a result of the noise analysis, the noise level at 1 Hz is set to a very low value such as $21\ pT\ /\ \sqrt{Hz}$.



(a) (b)

Figure 4.11 First generation UME Fluxgate magnetometer (a) Sensitivity (b) Noise measurements

The Earth's magnetic field has a different distribution on Earth due to the difference in underground resources. For this reason, global changes in the world's magnetic field have different effects depending on geography. Observations established in different regions around the world follow the annual magnetic field change in their region and contribute to determination of world magnetic field distribution by reporting the obtained scientific data. In order to obtain a healthy data, the accuracy of magnetic field measurements must be guaranteed. Sensitivity of devices used in magnetic field measurements to high sensitivity and environmental parameters is one of the parameters that must be absolutely necessary. The 1st Generation UME fluxgate magnetometer demonstrates robust design performance against environmental parameters. It has performed above expectations with the ability to solve even 1 nT DC field. It is expected that in 2014 there will be severe solar storms in September and December, which will cause magnetic field changes like 1000 nT, as is known from public announcements from many science centers (NASA, ESA, etc.) in the world. It has also been reported that such large DC field changes may have adverse effects on electronic devices. For this purpose, magnetic field measurements were made in the periods mentioned in a magnetically clean environment in the UME building and the DC field changes in this area were recorded. Figures (4.12) and (4.13) show the results of measurements made in September and December, respectively.

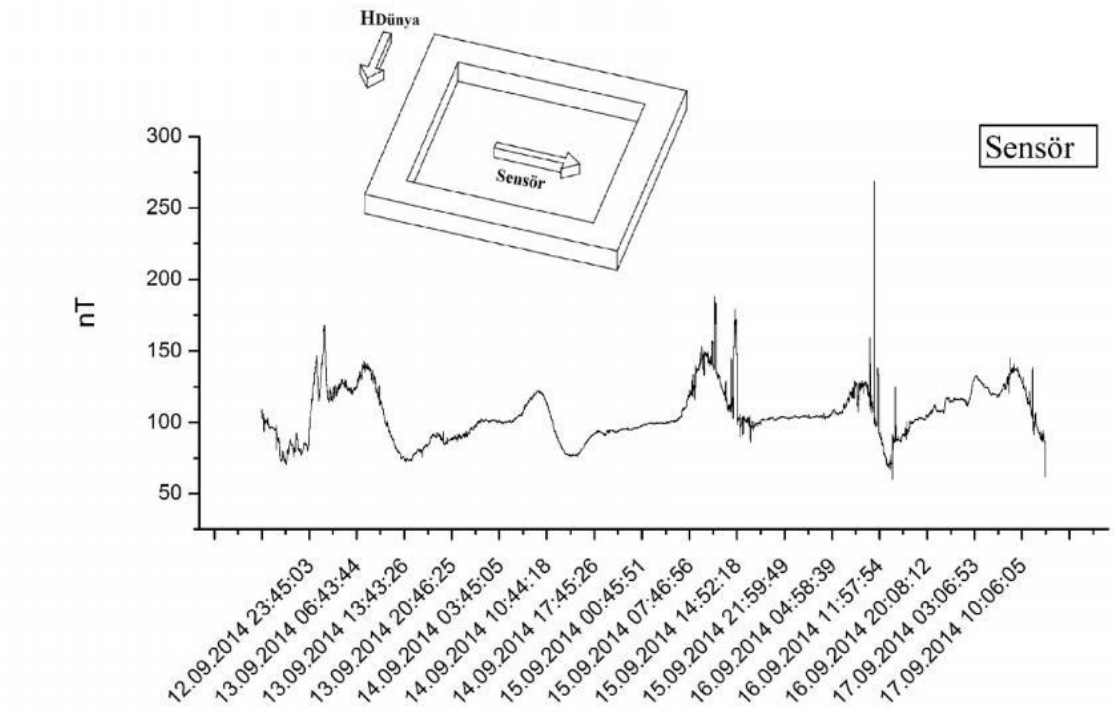


Figure 4.12 World magnetic field oscillations in the UME building controlled area from September 12 to 17

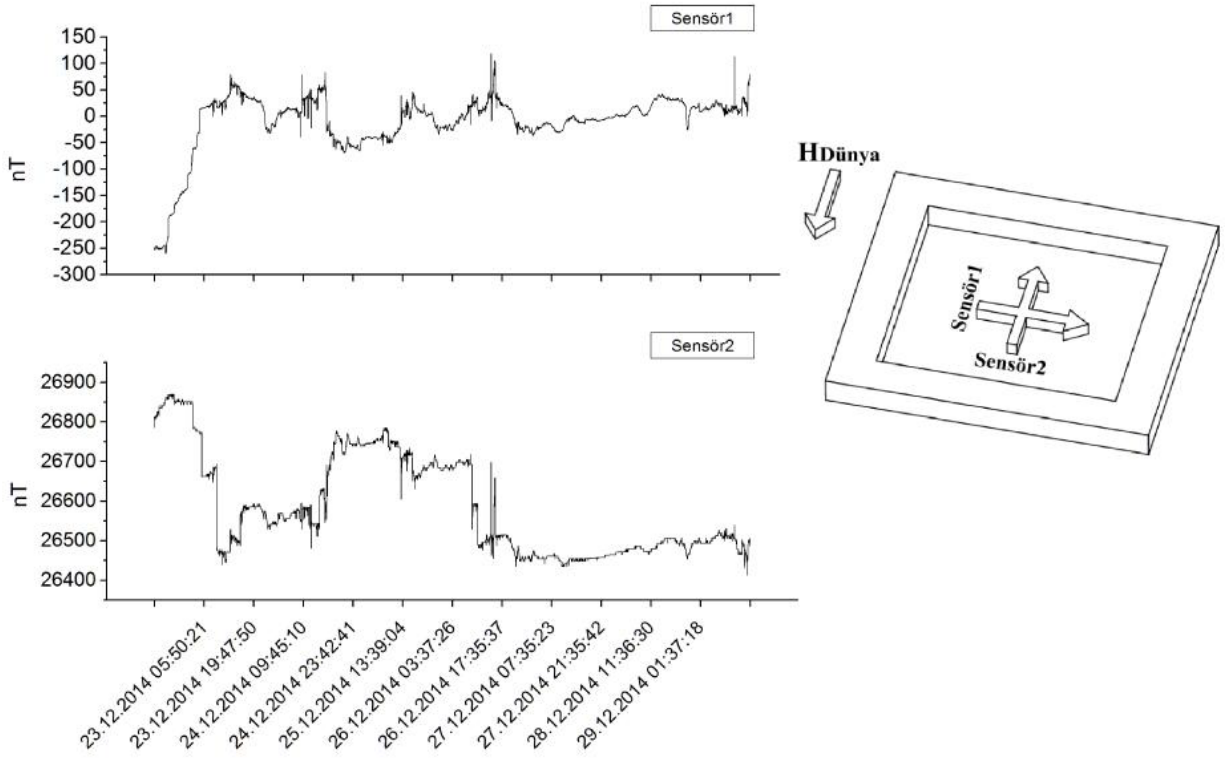


Figure 4.13 World Magnetic Field oscillations in the UME building controlled zone from December 21 to 29

Observational data graphs were compared with data from the Swedish Institute of Space Physics and the British Geological Survey 3, which were taken in real time and presented in open access. The daily change in the world magnetic field measurement in Figure (4.12) is between 100 and 200 nT in the UME building site, between 50 and 400 nT in IRF and between 50 and 250 nT in BGS. In the magnetic field measurement made in December, the daily change was between 50 and 200 nT, while between 200 and 450 nT in IRF and between 75 and 250 nT in BGS. It is seen that the solar storm, which many science centers expect from the dates in Figures (4.12) and (4.13), and where large earth magnetic changes in certain regions of the world can be observed, does not create the expected effect in these observatories. However, it is understood that there are different changes in the different regions of the world from the measurement results obtained. The magnetic field change in the records of the observatories located within the Swedish borders may be higher than in Turkey and the UK, but this difference may have been due to the fact that Sweden is closer to the northern polar region than the world.

CHAPTER 5

CONCLUSION AND FUTURE WORKS

In this study, Fluxgate magnetometer sensor and electronic circuit were designed and the Lock-In amplifier was studied. A one-dimensional magnetic field measurement was made while designing a fluxgate magnetometer. The drive signal used in the Fluxgate magnetometer is digital. In sinusoidal form, 1.086 kHz frequency and 1.31 V_{RMS} drive signal are used. Fluxgate sensor is selected and produced in ring core form. The input and output coils of the sensor were resonated and the maximum gain was achieved. The sensor was produced at TUBITAK UME Magnetic Laboratory. The direction of the magnetic field is detected by the phase detection technique from the detection signal representing the magnetic field. The amplitude of the magnetic field is also determined by integrating the detection signal. Produced magnetometer can measure with 1 mG accuracy. There is a perfect linear relationship between the DC field and the sensor output signal, which is of great metrological significance. On the other hand, as a result of the noise analysis, the noise level at 1 Hz is set to a very low value such as 21 $pT\sqrt{Hz}$. The result of this study is that the magnitude of the magnetic field in a single direction is measured by high performance over the earth and even the observation of the effect of a solar storm on earth magnetosphere has been achieved.

Fluxgate magnetometers have been used actively in the military field in the past, but nowadays commercial uses are spacecraft and satellites. With the fluxgate magnetometers placed on these vehicles, the orientations of the satellites are controlled after they are seated. In addition, special fluxgate magnetometers are being developed to study the magnetic field properties of our planet and other outer planets. If sufficient investment is made in space research in Turkey, it is one of the first satellite components that will be needed. Within the scope of the thesis, a

preliminary study has been carried out and the research has focused on the design of a magnetometer capable of working in space. It is also possible to use such magnetic sensors in the augmented reality world, which is another area that develops. Today, many portable personal computers are capable of generating position information with high accuracy, but they are open to serious developments in producing direction information. Fluxgate sensors with high precision and accuracy can be the solution for applications that are experiencing this lack of field.

REFERENCES

[1] Semiconductors, N., (2013). "Xtrinsic MAG3110 Three-Axis, Digital Magnetometer", http://www.nxp.com/assets/documents/data/en/data-sheets/MAG3110.pdf.

[2] Wikipedia, "Hall effect sensor", https://en.wikipedia.org/wiki/Hall_effect_sensor.

[3] Wikipedia, "SQUID superconducting quantum interference device", https://en.wikipedia.org/wiki/SQUID.

[4] Design, L.Q., "MPMS3 SQUID magnetometer", https://lot-qd.de/en/products/materials-science/magnetometers/product/mpms3-squid-magnetometer/.

[5] Wikipedia, "Vibrating sample magnetometer", https://en.wikipedia.org/wiki/Vibrating_sample_magnetometer.

[6] Technology, C.f.M.f.I., (2010). "DMS Vibrating Sample Magnetometer", http://mint.ua.edu/equipment/dms-vibrating-sample-magnetometer/.

[7] Djamal, M. ve Setiadi, R.N., (2009). "Development of fluxgate magnetometer using double cores probe".

[8] Sharafi, N. ve Nekoui, M.A., (2008). "Analyzing optimization of fluxgate sensor".

[9] London, I.C., "Fluxgate Magnetometers", http://www.imperial.ac.uk/space-and-atmospheric-physics/research/areas/space-magnetometer-laboratory/space-instrumentation-research/magnetometers/fluxgate-magnetometers/.

[10] INVASENS, (2006). "Rod Core Fluxgate", http://www.invasens.co.uk/fluxgate.html.

[11] INVASENS, (2006). "Ring Core Fluxgate", http://www.invasens.co.uk/fluxgate.html.

[12] Janosek, M., (2017). "Parallel Fluxgate Magnetometers", © Springer International Publishing Switzerland 2017.

[13] Ripka, P. ve Hurley, W.G., (2006). "Excitation efficiency of fluxgate sensors", Sensors and Actuators A: Physical, 129: 75-79.

[14] Mattia Butta, P.R., (2007). "Algorithm for Noise Reduction in Output Signal of Racetrack Core Fluxgate", PIERS ONLINE.

[15] Valery Korepanov, A.M., (2008). "MODERN FLUX-GATE MAGNETOMETERS DESIGN", MGB.

[16] Ripka, P. Janosek, M. Butta, M. Billingsley, S.W. ve Wakefield, E., (2009). "Crossfield effect in magnetic sensors".

[17] Petrucha, V. ve Kaspar, P., (2010). "Compact fluxgate sensor with a vector compensation of a measured magnetic field".

[18] Butta, M. Janosek, M. ve Ripka, P., (2010). "Coil-less fluxgate operated in feedback mode by means of dc current".

[19] Butvin, P. Janošek, M. Ripka, P. Butvinová, B. Švec Sr, P. Kuzminski, M. Švec Jr, P. Janičkovič, D. ve Vlasák, G., (2012). "Field annealed closed-path fluxgate sensors made of metallic-glass ribbons", Sensors and Actuators A: Physical, 184: 72-77.

[20] Mattia Butta, M.J., Pavel Ripka, Ludek Kraus, Rhimou El Kammouni, (2014). "Influence of Magnetostriction of NiFe Electroplated Film on the Noise of Fluxgate", IEEE Transactions on Magnetics Volume: 50.

[21] Son, H.H. Jung, I.I. Hong, N.P. Kim, D.G. ve Choi, Y.W., (2010). "Signal detection technique utilising 'lock-in' architecture using 2 ω_c harmonic frequency for portable sensors", Electronics Letters, 46: 891-892.

[22] Yang, Q., (2011). "Design and simulation of a lock-in amplifier".

[23] Leis, J. Martin, P. ve Buttsworth, D., (2012). "Simplified digital lock-in amplifier algorithm", Electronics Letters, 48: 259-261.

[24] Skillington, R.G., (2013). "DSP Based Lock-in Amplifier", University of Southern Queensland Faculty of Health, Engineering & Sciences.

[25] Kar, A. Chandra, M. Goel, P. ve Gupta, V.K., (2014). "A low-cost, portable alternative for a digital Lock-In Amplifier using TMS320C5535 DSP".

[26] Calangiu, D.I., (2014). "Implementation of a Digital Fluxgate Magnetometer for Nanosatellites", Luleå University of Technology Department of Computer Science, Electrical and Space Engineering.

[27] Butta, M. Sasada, I. ve Janosek, M., (2012). "Temperature Dependence of Offset and Sensitivity in Orthogonal Fluxgate Operated in Fundamental Mode", IEEE Transactions on Magnetics, 48: 4103-4106.

[28] Ripka, P. Pribil, M. ve Butta, M., (2014). "Fluxgate Offset Study", IEEE Transactions on Magnetics, 50: 1-4.

[29] Forslund, Å., (2006). "Designing a Miniaturized Fluxgate Magnetometer", Physical Electrotechnology Stockholm, April 2006.

[30] Ake Forslund, S.B., Nickolay Ivchenko, Goran Olsson, Terry Edberg1 and Andriy Marusenkov, (2007). "Miniaturized digital fluxgate magnetometer for small spacecraft applications", IOP PUBLISHING.

[31] Miles, D.M. Bennest, J.R. Mann, I.R. ve Millling, D.K., (2013). "A radiation hardened digital fluxgate magnetometer for space applications", Geosci. Instrum. Method. Data Syst., 2: 213-224.

[32] Hava Can, U.T., (2015). "Design of Ring Core Fluxgate Magnetometer as Attitude Control Sensor for Low and High Orbit Satellites", J Supercond Nov Magn.

[33] H.U. Auster, K.H.G., W. Magnes, O. Aydogar, W. Baumjohann, D. Constantinescu, D. Fischer, K.H. Fornacon, E. Georgescu, P. Harvey, O. Hillenmaier, R. Kroth, M. Ludlam, Y. Narita, R. Nakamura, K. Okrafka, F. Plaschke, I. Richter, H. Schwarzl, B. Stoll, A. Valavanoglou, M. Wiedemann, (2008). "The THEMIS Fluxgate Magnetometer", Space Sci Rev.

[34] K.-H. Glassmeiera, H.-U.A., D. Heynera, K. Okrafkaa, C. Carrb, G. Berghoferc, B.J. Andersone, A. Baloghb, W. Baumjohannc, P. Cargillb, U. Christensenf, M. Delvac, M. Doughertyb, K.-H. Fornaçona, T.S. Horburyb, E.A. Lucekb, W. Magnesc, M. Mandead, A. Matsuokah, M. Matsushimaj, U. Motschmanni, R. Nakamurac, Y. Naritaa, H. O'Brienb, I. Richtera, K. Schwingenschuhc, H. Shibuyak, J.A. Slaving, C. Sotinl, B. Stolla, H. Tsunakawaj, S. Vennerstromm, J. Vogtn, T. Zhangc, (2010). "The fluxgate magnetometer of the BepiColombo Mercury Planetary Orbiter", Planetary and Space Science, Volume 58: Pages 287–299.

[35] Laboratory, N.J.P., (2005). "https://saturn.jpl.nasa.gov/magnetometer/".

[36] Janosek, M. Platil, A. Vyhnanek, J. ve Brinek, J., (2013). "Dual-core fluxgate gradiometer with gradient feedback".

[37] Yang, X. Li, Y. Guo, W. Zheng, W. Xie, C. ve Yu, H., (2014). "A New Compact Fluxgate Current Sensor for AC and DC Application", IEEE Transactions on Magnetics, 50: 1-4.

[38] INSTRUMENTS, T., (2015). "DRV425 Fluxgate Magnetic-Field Sensor", Datasheet.

[39] D. Rühmer, S.B., F. Ludwig, (2015). "Vector Fluxgate Magnetometer for High Operation Temperatures up to 250°C", Sensors and Actuators A: Physical.

[40] Menghui Zhi, L.T., Xin Cao, Donghai Qiao, (2017). "Digital Fluxgate Magnetometer for Detection of Microvibration", Journal of Sensors, Volume 2017.

[41] Y.H. Pei, H.G.Y., (2009). "UXO Survey Using Vector Magnetic Gradiometer on Autonomous Underwater Vehicle", OCEANS 2009, MTS/IEEE Biloxi-Marine Technology for Our Future: Global and Local Challenges.

[42] BIZNETMALL, "METGLAS® MAGNETIC SHIELDING FILM", http://www.biznetmall.com/antiradiation/mag-shield.htm.

[43] Metglas®, I., "METGLAS® 2714A Cobalt Based Alloy ", Material Safety Data Sheet.

[44] Wikipedia, "A lock-in amplifier from Stanford Research Systems", https://en.wikipedia.org/wiki/Lock-in_amplifier.

CURRICULUM VITAE

PERSONAL INFORMATION

Name Surname : Sercan TANRISEVEN

Date of birth and place : 23.02.1991 / KIRKLARELİ

Foreign Languages : English

E-mail : f0513047@std.yildiz.edu.tr

EDUCATION

Degree	**Department**	**University**	**Date of Graduation**
Master			
Undergraduate	Electronics and Communication Engineering	Yildiz Technical University	27.01.2014
High School	Kırklareli Anatolian High School		

WORK EXPERIENCE

Year	**Corporation/Institute**	**Enrollment**
2015-Continuing	ERARGE	Hardware Engineer

PUBLISHMENTS

1. Sercan TANRISEVEN, Hava CAN, Uğur TOPAL, Cengiz BİRLİKSEVEN, Revna ACAR VURAL., "A low cost and simple fluxgate magnetometer implementation" , 2015 International Conference on Synthesis, Modeling, Analysis and Simulation Methods and Applications to Circuit Design (SMACD), 2015, İstanbul, Pages: 1 - 4, DOI: 10.1109/SMACD.2015.7301685